Characterization of Deodorized Kraft Lignin and Lignin-Polymer Composite Blends

A Thesis Presented for the
Master of Science
Degree
The University of Tennessee, Knoxville

Neel Jayantibhai Patel
December 2023

ACKNOWLEDGEMENTS

Dr. Dayakar Penumadu and Dr. David Harper played a crucial role in guiding me in this work. Dr. Philip Barnett played a major hands-on role in my development as a graduate researcher and student. Dr. Barnett provided guidance and led by example in terms of becoming a successful graduate student and researcher. Further acknowledgement is given to Andrew Patchen and Colby Gilbert for helping me in the lab. Andy Baker also played a crucial role in helping to prepare samples for mechanical testing. Many thanks to Prisma Renewable Composites, LLC for providing me with the opportunity to work on this project.

ABSTRACT

The aim of this work is to study different various softwood lignins and manufacture and characterize neat ABS-lignin composites. This involved characterizing deodorized and non-deodorized softwood lignins using techniques such as differential scanning calorimetry, thermogravimetric analysis, Fourier transform infrared spectroscopy, and principal component analysis. These techniques are used to determine the similarities and differences among the various softwood lignins at the functional group level. Neat ABS-lignin is blended in different weight fractions and analyzed for thermal and mechanical properties. A microscopic analysis of the blends is completed to study the interfacial properties of neat ABS-lignin. This effort was a collaboration among the Center for Renewable Carbon (CRC) and the Civil and Environmental Engineering Department, and Prisma Renewable Composites, LLC. The ABS-lignin blends showed a range of tensile strength of 33.0-40.6 MPa and a tensile modulus of 2.01-2.64 GPa. All ABS-lignin blends showed superior tensile and flexural strength and modulus, but showed lower impact resistance than neat ABS. These results are a result of the higher modulus of the lignin increasing the overall modulus and strength of the blends. The brittle nature of lignin reduces the impact resistance of the ABS-lignin blends as well as the ultimate strain. Microscopic analysis shows uneven spatial distribution of lignin in ABS resin.

TABLE OF CONTENTS

INTRODUCTION 1

CHAPTER 1: CHARACTERIZATION OF ODOR REDUCED SOFTWOOD KRAFT LIGNIN 3

CHAPTER 2: PHYSICAL, THERMAL, AND MECHANICAL EFFECTS OF DEODORIZED LIGNIN BLENDED IN ABS THERMOPLASTIC RESIN 23

APPENDIX 52

CONCLUSION 77

VITA 78

LIST OF TABLES

Table 1. CHNS elemental analysis of all lignin types. 53

Table 2. Assignment of lignin and their IR bands. 53

Table 3: P-NMR results (mmol OH/g lignin per sample)..... 53

Table 4. Decomposition temperature, glass transition temperature, and M_W..... 54

Table 5: Thermal data of ABS, lignin, and VF25..... 54

Table 6. TGA degradation study – degradation times. 54

Table 7: DMA and glass transition temperatures for ABS and ABS-L blends 55

Table 8. Tensile test results for ABS and ABS-L blends. 55

Table 9: Flexural test results for ABS and ABS-L blends..... 55

Table 10. Izod impact resistance for ABS and ABS-L blends. 56

Table 11: Average size of polybutadiene particles (μm^2)..... 56

LIST OF FIGURES

Figure 1. Structural units (monolignols) of lignin. 57

Figure 2. FTIR spectra for all lignin types. 57

Figure 3. PCA of all lignin types. 58

Figure 4. PC-1 loadings. 58

Figure 5. TGA and DTG curves for all lignin types. 59

Figure 6. TGA of VF25. 59

Figure 7. TGA degradation study – final weight remaining (%). 60

Figure 8. Tensile results of ABS-L blends 60

Figure 9. Flexural results of ABS-L blends. 61

Figure 10. Izod impact results of ABS-L blends. 61

Figure 11. Optical microscopy images of ABS, VF10, and VF35. 62

Figure 12. Nanoindentation elastic moduli. 63

Figure 13. Comparison of measured moduli with ROM moduli for VF10 and VF35. 63

Figure 14. Broadening of tanδ peaks. 64

INTRODUCTION

Lignin is a naturally occurring biopolymer that provides structural integrity to plant cell walls. Lignin is a highly abundant biomaterial, and it can be used as a raw material to create a variety of high-value products such as carbon fiber, biofuels, and various chemicals that are currently derived from petroleum. Lignin residue from the pulp and paper industry is primarily burned to provide energy. There is much research dedicated to lignin valorization. However, there are many challenges to converting lignin into commercial chemicals, materials, and fuels. Lignin has high degrees of branching, which creates highly variable and random structures. Additionally, the cross-linking in lignin molecules makes it difficult to modify lignin chemically. Another major challenge to using lignin for commercial products is the strong smell. Valmet, a Finnish technology supply company for the paper and pulp industry, has investigated odor reduction methods. Valmet has two patents for their guaiacol removal methods, the major contributor to the strong and unpleasant smell of lignin. However, before this odor-reduced lignin can be used for applications, the effect of the deodorization method on the lignin chemistry must be characterized. Chapter 1 focuses on comparing lignin from four softwood samples, two of which have undergone the deodorization process.

Lignin has been blended with various thermoplastics and thermoset materials. The high modulus lignin is expected to enhance mechanical properties in some materials. Blending lignin with such materials also makes them partially biodegradable. Therefore, blending low-cost lignin with common engineering plastics is a viable option. Acrylonitrile butadiene styrene (ABS) is an engineering plastic used in many common applications such as

automotive interiors. To develop an understanding of blending deodorized lignin with ABS, lignin was melt-blended with ABS, and the mechanical and thermal properties of the resulting blends were characterized. Chapter 2 focuses on analysis of these thermal and mechanical properties to better understand if deodorized lignin is a viable option for creating deodorized lignin-thermoplastic blends.

CHAPTER 1:
THERMAL, PHYSICAL, AND CHEMICAL CHARACTERIZATION OF ODOR REDUCED SOFTWOOD KRAFT LIGNIN

Authors: Neel J. Patel[A], Kendhl Seabright[B], Rebecca O'Toole[C], David P. Harper[B], Dayakar Penumadu[D]

[A]Department of Chemical Engineering, University of Tennessee, 232 Science and Engineering Research Facility, 1499 Circle Drive, Knoxville, TN 37916, USA

[B]Center for Renewable Carbon, University of Tennessee Institute of Agriculture, 2506 Jacob Drive, Knoxville, TN 37996, USA

[C]Department of Chemical Engineering, Penn State University, University Park, PA 16802, USA

[D]Department of Civil Engineering, University of Tennessee, 325 John D. Tickle Building, 851 Neyland Drive, Knoxville, TN 37996, USA

ABSTRACT

A major obstacle in the application of lignin in consumer products is the removal of volatile organic compounds and odor. Recent technology has produced a commercially viable odor-reduced lignin in hopes of making it viable for use in consumer products. This study will compare the odor reduced lignin to the non-odor reduced softwood kraft lignin samples obtained from different sources. The purpose of this study is to quantitatively determine differences in odor reduced and non-odor reduced kraft softwood lignin that would impact use by thermal, physical, and chemical characterization techniques. The characterization techniques are used to determine whether there has been odor reduction and whether the deodorization process has altered lignin chemistry and processability. The samples were taken from different geographical locations but were all LignoBoost kraft lignin from softwoods. The differences found between the samples are minimal. The greatest difference was found in the C-O-C stretching of the ether groups and C-O stretching of the G ring. Other differences observed are likely due to the differences in lignin due to the bio sources

from which they were extracted. Based on our thermal and chemical characterization, the properties and processability of odor-reduced lignin is very similar to non-odor reduced lignin, making it equally well-suited to be used for composite applications.

1. INTRODUCTION

1.1 Lignin Structure

Lignin makes up 20-35% of dry mass of wood, and it is the second most abundant biopolymer on the planet after cellulose (Boerjan et al. 2003). In plant cells, lignin provides structural support and resistance against microbial and oxidative degradation. The other main polymeric components of the wood cell wall are polysaccharides, cellulose and hemicelluloses. Lignin is composed of three monolignol units crosslinked in different ratios depending on botanical source. These monolignols are incorporated into lignin in the form of phenylpropanoids: guaiacyl (G), syringyl (S), and p-hydroxyphenyl (p-H) as shown in Figure 1 (all figures and tables are included in the Appendix at the end of the document). Softwood contains the highest percentage of lignin while hardwoods and grasses contain more polysaccharides.

The amounts of monolignol units vary greatly depending on botanical source, genetics, and other environmental factors that influence plant growth. Lignin composition and content are influenced by the species and also by the environment (Mandlekar et al. 2018a; Parit and Jiang 2020a). Softwood comes from gymnosperm trees such as pine and spruce. Lignin from softwoods contain almost exclusively guaiacyl units (Notley and Norgren 2009; Ralph et al. 2004).

1.2 Delignification Processes

There are a few types of delignification (separation of the lignin from hemicellulose and cellulose) or pulping processes used regularly in industry. Aside from the lignin source, the delignification method also plays an important role in the final structure of lignin. Delignification techniques, such as kraft, sulfite, and organosolv will also be considered in characterizing the lignin structure.

In the paper and pulp industry, the most used delignification process is called kraft pulping or sulfate process. In this process, wood chips are treated with a solution of sodium hydroxide and sodium sulfide at 150-180 °C (Wang et al. 2016). In this cooking liquor, lignin is fragmented by the anions through cleavage of alpha-ether and beta-aryl ether bonds, which increases the phenolic hydroxy groups in kraft lignin ("Gierer - Chemical aspects of kraft pulping" n.d.). Kraft lignin is typically recovered from the black liquor by precipitating under acidic conditions or by ultrafiltration. The kraft lignin process is a degradation process rather than a condensation process because the lignin is broken down into fragments while additionally enhancing dissolution from the source (Chakar and Ragauskas 2004). The natural, native lignin is degraded to vastly decrease the amount of polysaccharide bonds to the lignin. The lack of industrial applications is mainly attributed to the aliphatic thiol groups created during the kraft lignin process which give off a characteristic odor, more distinctly when heat treated.

1.3 Background

Industry leaders are looking to cut monetary and energy costs by finding alternative precursors and advancements in manufacturing. Environmental concerns and raw material

costs continue to drive the search for alternative polymer feedstocks for polyacrylonitrile (PAN), the precursor to carbon fiber, which is valued at $3,600/ton. A common polymer resin, acrylonitrile butadiene styrene (ABS) is valued at almost $2,000/ton (Gill et al. 2017; Ma et al. 2015). Because of lignin's significantly lower cost, valorization of lignin for carbon fiber composite applications would greatly reduce production costs. Lignin is appealing because of its biodegradability and abundance. Additionally, lignin in composites provides antioxidant properties (Domínguez-Robles et al. 2020) to prevent polymer aging (Pouteau et al. 2003; Pucciariello et al. 2004a). Lignin also produces a large amount of char residue, which reduces the flammability of polymers, and acts as a flame retardant by creating a physical charred barrier (Mandlekar et al. 2018a).

Kraft lignin, produced at 50 million tons annually, is a byproduct of the kraft pulping process used by majority of the paper and pulp industry (Mai et al. 2000a). The main use of this biopolymer byproduct is for combustion to supply energy back to the pulp plant. Lignin contains similar energy content to that of coal at 2.27 kJ/g, which is 30% more than cellulosic carbohydrates (Shafizadeh and Chin n.d.). Thus, the abundance of valuable carbon content in lignin is an untapped resource. As of 2017, kraft lignin is valued at $250/ton (Abbati De Assis et al. 2018). Giving value to what would otherwise be considered waste, lignin valorization research includes using lignin as a low-cost precursor to carbon fiber, engineering plastics, and various fuels and chemicals, which are currently sourced from petroleum (Bajwa et al. 2019a; Ragauskas et al. 2014a).

While the sulfite process produces lignosulfonates that have a wide variety of applications due to its water solubility, the industrial applications of kraft lignin, the dominant method of

producing wood pulp, has yet to be tapped. When using kraft lignin in composite materials or in other industrial or consumer applications, the odorous volatile organic compounds (VOCs) that occur naturally in the polymer must be reduced. VOCs have a high vapor pressure and will evaporate at room temperature. This leads to odors that plants use to communicate with other plants and animals. However, these same chemicals, including formaldehyde, benzene, and other complex substituted phenols, can be harmful or carcinogenic to human health. Odor reduced lignin has been heavily investigated by Valmet, the Finnish technology supply company for the pulp and paper industry. Generally, sulfurous compounds (dimethyl disulfide, dimethyl trisulfide, and dimethyl tetrasulfide) are thought to be the cause for the odor of lignin (*The next generation LignoBoost-tailor-maid lignin production for different lignin bioproduct markets* 2017a). Valmet has two patents ("Patent - Method of producing lignin with reduced amount of odorous substances" n.d.) for their guaiacol removal methods. Aside from guaiacol reduction, there are other differing characteristics present in the odor reduced lignin. Therefore, the effect of the deodorization process on lignin's chemical structure and the associated changes in physical and thermal properties must be characterized and understood. Valmet's odor reduction methods have made odor reduced lignin ready for commercialization for various end markets (*The next generation LignoBoost-tailor-maid lignin production for different lignin bioproduct markets* 2017a).

One commercial application of lignin has been offered by CycleWood Associates, LLC. One of their lignin-based products is Xylobags, which are compostable kitchen bags. Xylobags are melt-blown polyester films consisting of 30% lignin derivative (isolated via the

LignoBoost process) and a commercial biodegradable polyester (Glasser et al. 2017). However, several customer reviews of Xylobags reference the unpleasant smell of the bags. Insolubility of kraft lignin is also attributed to its lack of industrial applications. In order to incorporate kraft lignin into thermoplastics, for example, it must be mixed with a compatibilizer or chemically modified to ensure the lignin interacts and blends homogeneously into the resin (Akato, Tran, Chen, & Naskar, 2015). Studies have shown delignification processes increases the glass transition temperature by varying amounts (Sammons et al. 2013a). It is hypothesized that this increase is due to a change in chemical structure, functional group content, intermonomer bond type, and molecular size (Yang et al. 2019). If lignin were deodorized and compatibilized into thermoplastics such as acrylonitrile butadiene styrene (ABS), the applications for such lignin would be increased dramatically. Chemical, thermal, and physical characterization techniques are used in this study to understand the respective similarities and differences between odor reduced lignin and non-odor reduced lignin and how it may affect lignin's interactions with other polymers. Valmet's patent on the method of lignin deodorization indicates that the odor reduced lignin is mostly unchanged in its original molecular structure ("Patent - Method of producing lignin with reduced amount of odorous substances" n.d.). However, the deodorization process is known to remove more than 50% of guaiacol content from the lignin (*The next generation LignoBoost-tailor-maid lignin production for different lignin bioproduct markets* 2017a). Therefore, one goal of this study is to analyze how the deodorization process affects the chemical composition and chemical properties of odor reduced lignin. The chemical characterization techniques used in this study will help establish how any changes in lignin

chemical composition and structure may affect lignin's interaction with other polymers. The chemical characterization techniques used in this study include Fourier transform infrared spectroscopy (FTIR), principal component analysis (PCA), CHNS elemental analysis, and phosphorus NMR.

Any changes on the molecular composition of lignin will affect lignin's thermal properties. Also, for industrial applications, it is necessary to understand the thermal properties to determine optimal processing conditions for lignin. Thermal properties, such as decomposition temperature and glass transition temperature, are also studied, using techniques such as thermogravimetric analysis (TGA) and differential scanning calorimetry (DSC).

Physical characteristics of lignin are also studied to determine the size of the lignin molecules (in terms of molecular weight M_w) and moisture content. The size of the lignin molecules, along with its chemical composition, can affect lignin's blending properties with other polymers. The physical characterization techniques used in this study include gel permeation chromatography (GPC) and moisture content analysis.

2. MATERIALS AND METHODS

2.1 Lignin Samples

All softwood lignin samples used in this study were obtained from the LignoBoost kraft pulping process. Lignin samples L1 and L2 are deodorized samples, and samples L3 and L4 are non-deodorized samples; all four samples are commercial softwood kraft lignins. The lignin samples were provided by Prisma Renewable Composites, LLC. Therefore,

proprietary information regarding the exact source and pretreatments performed on the lignin samples are not provided. It is known that all four lignin samples are from a softwood source.

2.2 Thermogravimetric Analysis (TGA)

Thermogravimetric analysis (TGA) was used to characterize lignin decomposition in an inert environment using a Perkin Elmer Pyris 1 TGA. Lignin samples were heated in a nitrogen atmosphere from 25 to 800 °C at a rate of 10 °C/min. The lignin was held at 105 °C for 2 minutes to expel moisture from the sample. Weight loss of the lignin samples was recorded as the temperature increased to generate thermal decomposition curves. The first derivative of the thermal decomposition curve was used to determine the decomposition temperature of the lignin. TGA was repeated three times per lignin sample.

2.3 Differential Scanning Calorimetry (DSC)

Differential scanning calorimetry (DSC) was utilized to determine glass transition temperature (T_g) using a Perkin Elmer Diamond DSC. In a hermetically sealed pan, the lignin was heated from 30 to 160 °C during the first heat cycle, cooled to 30 °C, and then heated to 240 °C. All heating and cooling cycles were completed at a rate of 100 °C/min under a nitrogen atmosphere. The first heating cycle was used to expel any moisture or solvent from the sample and the second heating cycle was used to calculate Tg and heat capacity, Cp. DSC analysis was completed three times per lignin sample.

2.4 Fourier-Transform Infrared Spectroscopy (FTIR)

Fourier-Transform Infrared Spectroscopy (FTIR) measurements were collected for each lignin sample using a Perkin Elmer Spectrum One FTIR. Spectra were collected from 4000 –

600 cm^{-1} using 8 scans and a resolution of 4 cm^{-1}. Ten replicate spectra were collected for each lignin sample and were baseline corrected using the Spectrum One FTIR software.

2.5 Principal Component Analysis (PCA)

Principle component analysis (PCA) was accomplished by analyzing and comparing spectra from various lignin samples using the Unscrambler X software (Camo Analytics). The spectra were transformed in the software by several processing analyses required for PCA, including reduced average transformation, normalization, and extended multiplicative scatter correction (MSC/EMSC). Principle component loadings and scores were generated by the analysis to detail specific variances between the samples.

2.6 CHNS Elemental Analysis

Elemental analysis was performed by Atlantic Microlab (Norcross, GA) to determine the amount of carbon, hydrogen, nitrogen, and sulfur in each lignin sample. The sample was flash combusted at 1400 °C and transferred to a Perapak PQS column held at 60 – 80 °C using a Carlo Erba 1108 Elemental Analyzer. Elemental analysis data was collected in duplicate for each lignin sample.

2.7 Gel Permeation Chromatography (GPC)

Gel permeation chromatography (GPC) was used to determine molecular weight and polydispersity indices (PDI) of the lignin samples. Lignin was dissolved in tetrahydrofuran (THF) at a concentration of 1 mg/mL and filtered using a 0.2 µm PTFE syringe filter (Whatman). The sample (10 µL) was then injected into an EcoSEC GPC instrument at 40 °C setup with 3 columns (two Tosoh TSKgel SuperMultiporeHZ-M (4.6×150 mm; 4 µm) and a

TSKgel SuperMultiporeHZ-M guard column). THF was used as the mobile phase at 0.35 mL/min and a RI detector was utilized. A polystyrene (PS) standard was used to calibrate the instrument and the sample chromatograms were analyzed using the EcoSEC software.

3. RESULTS AND DISCUSSION

Thermal, chemical, and physical techniques were used to characterize four kraft lignin samples, two odor-reduced and two non-odor reduced. Lignin samples L1 and L2 are both odor-reduced samples. Samples L3 and L4 are non-odor reduced samples. The goal of this study is to distinguish if, by the attempted techniques, any similarities or differences can be established between odor reduced and non-odor reduced lignin.

3.1 Elemental Analysis

The most abundant component in lignin is carbon. The carbon and hydrogen content remains relatively similar among all samples. L1 and L2, the deodorized samples, are devoid of nitrogen and contain less sulfur than the non-treated lignin samples, L3 and L4. This result agrees with Valmet's analysis of the source of smell in lignin. Previous to Valmet's olfactometric analysis, sulfurous compounds, such as dimethyl disulfide, dimethyl trisulfide, and dimethyl tetrasulfide, were thought to be the main source of smell from lignin (*The next generation LignoBoost-tailor-maid lignin production for different lignin bioproduct markets* 2017a). Contrarily, Valmet's analysis shows that guaiacol and ethyl guaiacol are the main contributors of lignin odor. This CHNS analysis shown in Table 1, shows a decrease in sulfur content. The guaiacol content measured by NMR indicates effectiveness of the deodorization process.

3.2 Chemical Characterization

3.2.1 FTIR Analysis

The stretches labeled in Figure 3 are all related to the S and G rings. L1 and L3 seem to have more drastic stretching than L2 and L4, most notably at wavelengths 1267 cm-1 and 1212 cm-1. Both 1267 cm-1 and 1212 cm-1 correspond to the G ring (Table 2). Overall, the spectra all resemble each other closely. More specifically, it is observed that L1 and L3 are chemically similar, although L1 is deodorized and L3 is not. This may be due to the origin of samples being from a similar source. Based on this, it can be concluded that there are no significant observed chemical differences between the deodorized and non-deodorized lignin samples. Principal component analysis (PCA) was performed on these spectra to visualize the differences. (Watkins et al. 2015).

3.2.2. PCA Analysis

The PCA scores plot is shown in Figure 3 with 10 replicates of each of the 4 lignin samples. PCA is a statistical method used to compare samples and visually show where the differences lie. The overall range of the PCs and difference in grouping is rather small. Three distinct clusters are observed in the scores plot (Figure 3): the L1/L3 cluster, L2 cluster, and L4 cluster. PC-1 represents 67% of the total variance observed among the samples. Along the PC-1 axis, L1 and L3 are grouped closely together, indicating that they have similar chemical compositions. Combined with their similar FTIR spectra, the grouping of L1 and L3 on the scores plot further shows their similarity. As their FTIR spectra closely resemble each other, their differences are likely due to the origins of the samples being from different softwood

sources. The major differences are between L2 and L4 along the PC-1 axis, making them the most dissimilar pair. L1 has a relatively large spread across PC-1 axis, signifying differences in each replicate of that sample.

The PC-1 loadings, shown in Figure 4, signify the areas of the FTIR spectra that lead to the largest differences. Since PC-1 showed the largest differences in the lignin samples, the peaks have been assigned in Table 2. The structure causing the largest variation between the lignin samples is at peak 1047 cm^{-1}, which corresponds to the C-O-C ether groups, which are prevalent between lignin monomer units. According to Valmet, guaiacol is the main component responsible for the odor. In their deodorization process, the removal of the G ring results in the reduction of C-O-C ether bonds, which causes the large peak at 1047 cm^{-1}. The 1139 cm^{-1} peak is from the C-H stretching of the G ring. The G ring is removed during the deodorization process, causing the relatively large peak. Although these differences were detected, the magnitude of the differences is very small, indicating that all four lignin samples are very similar in composition.

PC-2 accounts for only 13% of the variance among the samples. As observed in Figure 3, all samples are grouped closely together along the PC-2 axis. The 13% variance is largely caused by the large spread due to the two outlier replicates of the L1 sample.

3.3 Thermal Characterization

3.3.1 Decomposition Temperature

Decomposition and glass transition temperature are both dependent on the molecular structure of the sample. According to Watkins et al., there are three temperature ranges where

different kinds of weight loss occur in lignin samples (Watkins et al. 2015). The first stage is between 30-120℃ where any moisture held by the lignin is evaporated. The second stage is from 180-350℃, where the degradation of carbohydrates and the lignin sample occurs, leading to release of volatiles such as CO, CO_2, and CH_4. Additionally, a study by Liu et al. (Liu et al. 2008) showed the formation of several phenolic groups such as 2-methoxyphenol (guaiacol), 2,6-dimethoxyphenol (syringyl), and 2-methoxy-4-alkyl substituted phenols in the 220-230℃ range. Note that guaiacol, the main source of lignin odor according to Valmet's olfactometric analysis, is removed in the second stage (*The next generation LignoBoost-tailor-maid lignin production for different lignin bioproduct markets* 2017a). The final stage is above 350℃ where more volatiles derived from phenolics, alcohols, and aldehyde acids are released. Watkins et al. concluded that the thermal properties of lignin are in fact dependent upon the lignin source (Watkins et al. 2015).

Table 4 shows the decomposition temperatures of each sample tested. L1 has the highest decomposition temperature, while L2, L3, and L4 had similar decomposition temperatures. L1's higher decomposition temperature may be attributed to the deodorization process. Although the exact source of the lignin is unknown, all of the samples are derived from softwoods, and it is known that L1 and L2 came from different sources. The difference in source location could also have contributed to L1 having a 20℃ higher decomposition temperature than the others. Figure 5 graphs all the TGA data recorded for each sample. There was a spike in DTG curves for all samples at approximately 100°C, indicating moisture loss.

3.3.2 Glass Transition Temperature

The glass transition temperature of the samples range from 140-155℃ (Table 4). Based on existing literature, the range of the T_g observed in Table 4 is standard for kraft lignin. None of the samples tested fall outside the expected range of 140-160℃ for softwood lignin (Kubo and Kadla 2005; Kun and Pukánszky 2017). As shown in Table 4, L1 also has the highest T_g, and this may be due to higher crosslinking in the sample. L4's low glass transition temperature can be largely attributed to the low Mn. Due to the shorter polymer chains, L4 has a higher free volume, which leads to increased chain mobility, resulting in a lower glass transition temperature.

4. CONCLUSION

In this study, we examined the deodorized softwood lignin samples with non-deodorized softwood lignin samples obtained from the Kraft pulping process. The differences found between the samples are minimal. The most significant differences occur due to the softwood lignin sources being from different geographical locations. This indicates there are other characterization techniques that must be explored to find the characterizable differences between the species. Minor differences were observed in the elemental analyses of the samples, namely the sulfur content. The noticeable difference between the deodorized samples and non-deodorized samples is the C-O-C stretching of the ether groups and C-O stretching of the G ring due to the removal of guaiacol and 4-ethyl guaiacol units during the deodorization process; however, the magnitude of this difference is rather small. This means that the deodorization process does not significantly change the overall structure and formation of the lignin. This is beneficial because techniques and polymer to resin binding

systems will work equally well on the odor reduced kraft lignin as the non-odor reduced kraft lignin.

REFERENCES

[1] Boerjan W, Ralph J, Baucher M. Lignin Biosynthesis. Annu Rev Plant Biol 2003;54:519–46. https://doi.org/10.1146/annurev.arplant.54.031902.134938.

[2] Tejado A, Peña C, Labidi J, Echeverria JM, Mondragon I. Physico-chemical characterization of lignins from different sources for use in phenol-formaldehyde resin synthesis. Bioresour Technol 2007;98:1655–63. https://doi.org/10.1016/j.biortech.2006.05.042.

[3] Mandlekar N, Cayla A, Rault F, Giraud S, Salaün F, Malucelli G, et al. An Overview on the Use of Lignin and Its Derivatives in Fire Retardant Polymer Systems. Lignin - Trends and Applications, InTech; 2018. https://doi.org/10.5772/intechopen.72963.

[4] Parit M, Jiang Z. Towards lignin derived thermoplastic polymers. Int J Biol Macromol 2020;165:3180–97. https://doi.org/10.1016/j.ijbiomac.2020.09.173.

[5] Ralph J, Lundquist K, Brunow G, Lu F, Kim H, Schatz PF, et al. Lignins: Natural polymers from oxidative coupling of 4-hydroxyphenyl- propanoids. Phytochemistry Reviews 2004;3. https://doi.org/10.1023/B:PHYT.0000047809.65444.a4.

[6] Notley SM, Norgren M. Lignin: Functional Biomaterial with Potential in Surface Chemistry and Nanoscience. The Nanoscience and Technology of Renewable Biomaterials, 2009. https://doi.org/10.1002/9781444307474.ch7.

[7] Wang C, Kelley SS, Venditti RA. Lignin-Based Thermoplastic Materials. ChemSusChem 2016;9. https://doi.org/10.1002/cssc.201501531.

[8] Gierer - Chemical aspects of kraft pulping n.d.

[9] Chakar FS, Ragauskas AJ. Review of current and future softwood kraft lignin process chemistry. Ind Crops Prod, vol. 20, 2004, p. 131–41. https://doi.org/10.1016/j.indcrop.2004.04.016.

[10] Gill AS, Visotsky D, Mears L, Summers JD. Cost Estimation Model for Polyacrylonitrile-Based Carbon Fiber Manufacturing Process. Journal of Manufacturing Science and Engineering, Transactions of the ASME 2017;139. https://doi.org/10.1115/1.4034713.

[11] Ma Z, Weersink A, Vadori R, Misra M. Financial cost comparison of acrylonitrile butadiene styrene (ABS) and BioABS. J Biobased Mater Bioenergy 2015;9. https://doi.org/10.1166/jbmb.2015.1520.

[12] Domínguez-Robles J, Larrañeta E, Fong ML, Martin NK, Irwin NJ, Mutjé P, et al. Lignin/poly(butylene succinate) composites with antioxidant and antibacterial properties for potential biomedical applications. Int J Biol Macromol 2020;145. https://doi.org/10.1016/j.ijbiomac.2019.12.146.

[13] Pouteau C, Dole P, Cathala B, Averous L, Boquillon N. Antioxidant properties of lignin in polypropylene. Polym Degrad Stab 2003;81:9–18. https://doi.org/10.1016/S0141-3910(03)00057-0.

[14] Pucciariello R, Villani V, Bonini C, D'Auria M, Vetere T. Physical properties of straw lignin-based polymer blends. Polymer (Guildf) 2004;45:4159–69. https://doi.org/10.1016/j.polymer.2004.03.098.

[15] Mai C, Milstein O, Hü A. Chemoenzymatical grafting of acrylamide onto lignin. vol. 79. 2000.

[16] Shafizadeh F, Chin PPS. Thermal Deterioration of Wood. n.d.

[17] Abbati De Assis C, Greca LG, Ago M, Balakshin MY, Jameel H, Gonzalez R, et al. Techno-Economic Assessment, Scalability, and Applications of Aerosol Lignin Micro- and Nanoparticles. ACS Sustain Chem Eng 2018;6:11853–68. https://doi.org/10.1021/acssuschemeng.8b02151.

[18] Bajwa DS, Pourhashem G, Ullah AH, Bajwa SG. A concise review of current lignin production, applications, products and their environment impact. Ind Crops Prod 2019;139. https://doi.org/10.1016/j.indcrop.2019.111526.

[19] Ragauskas AJ, Beckham GT, Biddy MJ, Chandra R, Chen F, Davis MF, et al. Lignin valorization: Improving lignin processing in the biorefinery. Science (1979) 2014;344. https://doi.org/10.1126/science.1246843.

[20] The next generation LignoBoost-tailor-maid lignin production for different lignin bioproduct markets. 2017.

[21] Patent - Method of producing lignin with reduced amount of odorous substances n.d.

[22] Glasser WG, Loos R, Cox B, Cao H. Melt-blown compostable polyester films with lignin. Tappi J 2017;16. https://doi.org/10.32964/tj16.3.111.

[23] Sammons RJ, Harper DP, Labbé N, Bozell JJ, Elder T, Rials TG. Organosolv lignin analysis. vol. 8. 2013.

[24] Yang J, Ching YC, Chuah CH. Applications of lignocellulosic fibers and lignin in bioplastics: A review. Polymers (Basel) 2019;11. https://doi.org/10.3390/polym11050751.

[25] Watkins D, Nuruddin M, Hosur M, Tcherbi-Narteh A, Jeelani S. Extraction and characterization of lignin from different biomass resources. Journal of Materials Research and Technology 2015;4. https://doi.org/10.1016/j.jmrt.2014.10.009.

[26] Liu Q, Wang S, Zheng Y, Luo Z, Cen K. Mechanism study of wood lignin pyrolysis by using TG-FTIR analysis. J Anal Appl Pyrolysis 2008;82:170–7. https://doi.org/10.1016/j.jaap.2008.03.007.

[27] Kubo S, Kadla JF. Kraft lignin/poly(ethylene oxide) blends: Effect of lignin structure on miscibility and hydrogen bonding. J Appl Polym Sci 2005;98:1437–44. https://doi.org/10.1002/app.22245.

[28] Kun D, Pukánszky B. Polymer/lignin blends: Interactions, properties, applications. Eur Polym J 2017;93:618–41. https://doi.org/10.1016/j.eurpolymj.2017.04.035.

CHAPTER 2:
THERMAL AND MECHANICAL CHARACTERIZATION OF REDUCED ODOR SOFTWOOD KRAFT LIGNIN BLENDED IN ABS THERMOPLASTIC RESIN

Authors: Neel J. Patel[A], Philip Barnett, David Harper[B], Dayakar Penumadu[C]

[A]Department of Chemical Engineering, University of Tennessee, 232 Science and Engineering Research Facility, 1499 Circle Drive, Knoxville, TN 37916, USA

[B]Center for Renewable Carbon, University of Tennessee Institute of Agriculture, 2506 Jacob Drive, Knoxville, TN 37996, USA

[C]Department of Civil Engineering, University of Tennessee, 325 John D. Tickle Building, 851 Neyland Drive, Knoxville, TN 37996, USA

ABSTRACT

A growing need exists to increase sustainability of bulk thermoplastics. Lignin appears to be an ideal candidate as it is produced in large quantities, has high carbon content, and has low cost. However, adding lignin from the kraft process into thermoplastics usually degrades toughness and strength of the blend and gives off what many think is an unpleasant odor. We incorporated a novel deodorized kraft lignin with acrylonitrile butadiene styrene (ABS) thermoplastic resin. ABS resin and lignin powder were manually blended and pelletized for injection molding into mechanical test specimens. The mechanical and thermal properties of the resulting ABS/lignin blends are presented, with optical microscopic analysis providing further insight. The tanδ value decreased with increasing lignin loading, indicating the material's decreased ability to dissipate energy upon impact. Both the tensile and flexural moduli increased upon lignin addition due to lignin's reinforcing effect. Optical microscopy images show the agglomeration of lignin particles in VF35, which shows poor miscibility between lignin and ABS. Deodorized lignin acts as a filler in ABS. Therefore, it is best to formulate ABS-lignin blends with a lower lignin weight fraction for commercial applications.

1. INTRODUCTION

1.1 Background

Lignin is the second most abundant biopolymer on earth after cellulose (Boerjan et al. 2003). For example, more than 50 million tons of kraft lignin is produced by the paper and pulp industry(Mai et al. 2000b; *The next generation LignoBoost-tailor-maid lignin production for different lignin bioproduct markets* 2017a), and majority of this lignin is combusted to supply energy. This study focuses on lignin obtained from the kraft pulping process. Kraft pulping is the most common method in the paper and pulp industry, consisting of almost 90% of total chemical wood pulp production (Marquardt et al. 2010; Tran and Vakkilainnen 2012). In kraft pulping, the wood chips are cooked with sodium hydroxide and sodium sulfide at 150-180 °C (Wang et al. 2016), where the liquid phase becomes a slurry of mostly lignin and some hemicellulose. In the paper and pulp industry, 98% of the slurry, or black liquor, is burned for energy recovery (Bajwa et al. 2019b; Ragauskas et al. 2014b). To improve the economic viability of pulp production, lignin valorization is of interest. For example, lignin can help reduce the carbon footprint because it allows the replacement of hydrocarbon-derived polymers with a naturally derived alternative. The composition of lignin is dependent upon the raw material source and the delignification method (Mandlekar et al. 2018b). Overall, lignin molecules have high degrees of branching, random structures, and cross-linking, making lignin difficult to modify chemically.

Lignin's aromatic structure lends itself to multiple decomposition products that are considered pleasant to unpleasant to the human nose, such as vanillin and guaiacol. Lignin naturally has a sulfuric odor due to the formation of byproducts in the Kraft pulping process.

In the process, lignin is broken down into byproducts, creating sulfur derivatives such as sulfides, sulfates, thiols, and monomeric aromatic alcohols (Lu and Gu 2022). Valmet has engineered a treatment that reduces the lignin odor so that it can be incorporated into resins for industrial applications (*The next generation LignoBoost-tailor-maid lignin production for different lignin bioproduct markets* 2017a). A characterization study completed by Patel et. al. discovered that there is no significant difference between the Valmet process and non-odor reduced lignin with regards to thermal or chemical properties. As such, it is possible to use deodorized lignin for consumer products as it does not lose any significant properties after undergoing Valmet's lignin deodorization process. Since the lignin odor problem has been addressed, it is important to evaluate the ability of deodorized lignin to be incorporated into thermoplastic resin systems.

The biodegradability, availability, abundance, and low cost of lignin can be exploited via polymer blending to create composites with potentially enhanced mechanical properties due to lignin's high modulus (Parit and Jiang 2020b). However, there are challenges associated with blending lignin with other polymers/thermoplastics (Kadla and Kubo 2004; Parit and Jiang 2020b; Song et al. 2012). The extensive cross-linking and strong intramolecular interactions make lignin difficult to melt process (Parit and Jiang 2020b). As such, it is difficult to create thermoplastic-lignin blends with greater than 20-30% wt% (Li et al. 1997; Parit and Jiang 2020b). Thermal analyses indicate that lignin is not miscible in blends containing PVA and PP, but it was found to be miscible in PEO and PET blends (Kadla and Kubo 2004). Many of these blends are created using conventional melt-mixing used for thermoplastics (Pucciariello et al. 2004b). To improve lignin miscibility in polymer blends,

several studies indicate the use of chemical compatibilizers such as maleic anhydride grafted styrene-ethylene/butylene-styrene (SEBS-g-MA) and polyethylene oxide (PEO) to improve interfacial adhesion (Akato et al. 2015; Pucciariello et al. 2004b; Song et al. 2012). Furthermore, some studies have examined lignin modifications to enhance miscibility and processability of lignin-thermoplastic blends. Thielemans and Wool concluded that butyrated kraft lignin is soluble in styrene, a nonpolar compound (Thielemans and Wool 2005). Other lignin modification studies have shown that acetylated and methylated lignin is soluble in non-polar thermoplastic polymers (Kim et al. 2017; Nevrez et al. 2011), and it also reduces T_g of the modified lignin, enabling better flow properties (Cachet et al. 2014; Lisperguer et al. 2009). To maximize reducing the carbon footprint, lignin content must be maximized in polymer blends without compromising the thermal and mechanical properties of the material. Various studies have examined lignin-thermoplastic blends. Song et. al. concluded that incorporating 5 wt% lignin into ABS increases the tensile strength by 2 MPa and modulus by 0.1 GPa; higher lignin loadings were shown to decrease mechanical properties (except for modulus), but that issue can be solved by reactive compatibilization (Song et al. 2012). Similarly, another study conducted by Akato et. al. at Oak Ridge National Laboratory found that adding 10 wt% lignin in ABS increases the relative (as compared to the neat ABS matrix) tensile strength by approximately 10% and relative modulus by approximately 20%; again, higher lignin loadings drastically decreased the mechanical properties, except for modulus (Pucciariello et al. 2004b). Furthermore, they discovered that composites made of carbon fiber and a polymer blend of ABS/lignin/PEO showed slightly increased mechanical properties compared to composites with a polymer blend of ABS/lignin (Akato et al. 2015).

1.2 Lignin and Acrylonitrile Butadiene Styrene (ABS) Chemistry

Many studies on lignin-thermoplastic blends have been reported in literature. Lignin has been blended with polyethylene (Alexy et al. 2004, n.d.) (PE), polypropylene (Alexy et al. n.d.; González Sánchez and Expósito Alvarez 1999) (PP), polylactic acid (PLA) (Li and Chua 2003), and polybutylene succinate (Sahoo et al. 2011) (PBS). In many cases, the tensile strength of the blends decreased with the addition of lignin (Alexy et al. n.d.; González Sánchez and Expósito Alvarez 1999; Li and Chua 2003). For the PLA-lignin blend, the Young's modulus also decreased after the addition of lignin (Li and Chua 2003). In the case of PE and PBS, the addition of ethylene-vinylacetate as a modifier and polymeric methylene diphenyl diisocyanate as compatibilizer, respectively, improved the tensile strength of the blends (Alexy et al. 2004; Sahoo et al. 2011). It would be ideal to use 100% biodegradable or green thermoplastics for commercial applications; however, there are still major challenges associated with this route. For example, PHAs (polyhydroxyalkanoates), which are a group of natural biodegradable polyesters, are synthesized by microorganisms and are fully biodegradable ("Li - Polyhydroxyalkanoates - opening doors for a sustainable future" n.d.). PHAs tend to have poor mechanical properties, higher production cost, and are less compatible with conventional thermal processing techniques ("Li - Polyhydroxyalkanoates - opening doors for a sustainable future" n.d.). In this study, acrylonitrile butadiene styrene (ABS) was chosen as the thermoplastic resin. ABS is a good thermoplastic candidate for lignin for several reasons. For one, ABS is a widely used thermoplastic for engineering applications as it possesses a good balance of mechanical properties, good chemical resistance, and high impact resistance (Akato et al. 2015; Song et al. 2012). Both ABS and

lignin have aromatic rings in their chemical structure. ABS has polar -CN groups in its polymer chain, while lignin has polar -OH groups. Both lignin and ABS also possess aromatic rings in their structure, which can also lead to weak nonpolar interactions between the two materials. Thus, due to similarities in their chemical structure, ABS and lignin are expected to exhibit interfacial compatibility (Song et al. 2012). Blending lignin with ABS will also make the resulting thermoplastic partially biodegradable (Song et al. 2012).

2. MATERIALS AND METHODS

2.1 Acrylonitrile Butadiene Styrene (ABS)

The ABS resin used in this study is Magnum™ 3325 MT manufactured by Trinseo. Magnum™ is typically used in automotive applications (Magnum datasheet). The advantages of Magnum™ resin include low VOC content, good heat stability, and high scratch and mar resistance. The reported nominal density of the ABS resin is 1.05 g/cm^3, and preliminary experiments found a density of 1.0387 g/cm^3 for the as-received pellets. The tensile modulus is 2.20 GPa, and the tensile strength is 43.0 MPa at a strain of 3.3%. The flexural modulus is 2.10 GPa, and the flexural strength is 65.0 MPa. The notched Izod impact strength of the ABS resin is 17 kJ/m^2.

2.2 Lignin

The lignin samples were provided by Prisma Renewable Composites, LLC. Proprietary information regarding the exact source and pretreatments performed on the lignin sample is not provided. The softwood lignin used in this study has been extracted from the LignoBoost kraft pulping process. Additionally, the lignin has been deodorized using Valmet's

process(*The next generation LignoBoost-tailor-maid lignin production for different lignin bioproduct markets* 2017b). Lignin was used as received with only additional drying at 80°C for 24 hours. The T_g of the lignin used in this study is 155 °C.

2.3 Lignin Fibers

Indulin AT softwood kraft lignin was obtained from MeadeWestvaco (now WestRock). The lignin was washed and filtered with deionized water until the water appeared clear. The washed lignin material was then extracted by adding the lignin to methanol at a ratio of 10:1 (methanol to lignin), covered, and stirred overnight at room temperature. The material was then filtered through Whatman Grade 1 filter using a Buchner funnel attached to a vacuum flask. The material in the solution was recovered by evaporating the methanol on a rotary evaporator (Buchi). The lignin was scraped from the flask and dried at 65 °C for 48 hours in a vacuum oven at 22 in Hg.

Fibers were produced by melt spinning in a custom Alex James and Sons single screw extruder (12.5 mm diameter) equipped with an HPB-5556-0.297-000 Zenith gear pump (0.297 cc/rotation) and a 12 x 150 µm diameter spinneret. The fibers were extruded at a pressure of 400 psi (2.76 MPa) at 195 °C. Fibers were collected at a rate of 300 m/min. The resulting 100% lignin fibers were not subjected to any thermal treatment.

2.4 Extrusion

The ABS resin and lignin powder were hand-blended and slowly poured into the extruder. A Leistritz ZSE Maxx 27 (27 mm parallel twin screw) extruder with a barrel length to diameter of 40:1 and a speed of 1200 rpm was used to obtain blended ABS-L pellets with various

lignin weight fractions. Prisma Renewable Composites LLC determined the proprietary blending and extrusion process parameters. It was reported that the processing conditions used for the blends were in the typical processing range for ABS resin.

2.5 Injection Molding

The neat ABS and ABS-L samples were injection molded at the Polymer Center of Excellence in Charlotte, NC. The samples were manufactured in a multi-cavity Arburg 320A press using typical processing conditions for neat ABS. Prisma Renewable Composites LLC determined the proprietary injection molding process parameters. ASTM D638 ("Standard Test Method for Tensile Properties of Plastics 1" n.d.) Type I dog-bone tensile specimens and ASTM D790 ("Standard Test Methods for Flexural Properties of Unreinforced and Reinforced Plastics and Electrical Insulating Materials 1" n.d.) flexural specimens were molded and tested. ASTM D256 ("D256 - Izod Impact Testing for Plastics" n.d.) Izod impact specimens were obtained by cutting the flexural specimens to the appropriate length prior to notching.

2.6 Thermogravimetric Analysis (TGA)

Thermogravimetric analysis (TGA) was used to characterize ABS-L decomposition in an inert environment using a Perkin Elmer Pyris 1 TGA. Lignin samples were heated in a nitrogen atmosphere from 25 to 800 °C at a rate of 10 °C/min. The lignin was held at 105 °C for 2 minutes to expel moisture from the sample. Weight loss of the lignin samples was recorded as the temperature increased to generate mass loss curves. The first derivative of the

mass loss curve was used to determine the decomposition temperature of the lignin. TGA was repeated three times per lignin sample.

A separate TGA degradation study was also conducted. Samples heated to and held isothermally from 180-230 °C at 10 °C increments for 30 minutes to determine the rate of degradation. This study was completed for neat ABS, VF10, and VF35 samples. The TGA degradation study was also conducted in an inert environment.

2.7 Differential Scanning Calorimetry (DSC)

Differential scanning calorimetry (DSC) was used to determine glass transition temperature (T_g) using a TA Instruments DSC Q2000. In a hermetically sealed pan, the lignin was heated from 30 °C to 160 °C during the first heat cycle, cooled to 30 °C, and then heated to 240 °C. All heating and cooling cycles were completed at a rate of 20°C/min under a nitrogen atmosphere. The first heating cycle was used to expel any moisture or solvent from the sample, and the second heating cycle was used to calculate T_g. The first cycle also served to eliminate any previous thermal history of the sample. DSC analysis was completed three times for neat ABS, VF10, and VF35.

2.8 Dynamic Mechanical Analysis (DMA)

Dynamic mechanical analysis (DMA) was used to determine the glass transition temperature using a Perking Elmer Diamond DMA. Each sample was tested from 25-140 °C with a heating rate of 2°C/min. The samples were tested in a dual-cantilever bending mode at 1 Hz frequency with a deformation limit of 20μm. Three specimens were tested for neat ABS, VF10, and VF35.

2.9 Tensile Testing

Tensile tests were completed with Type I specimens at room temperature using the ASTM D638 standard. The dimensions for the tensile specimens were 12.67 mm x 3.09 mm x 57 mm. The testing was completed using the MTS 858 load frame with a 25 kN load cell. An extensometer was used in the gauge region. A gripping pressure of 400 psi (2.75 MPa) was used to grip the specimens. The samples were tested at a crosshead rate of 5 mm/min. Tensile testing was completed for neat ABS and ABS-lignin blends; tensile testing could not be completed on the lignin fibers as the fibers were too fragile to handle.

2.10 Flexural Testing

Three-point bending flexural tests were completed using the ASTM D790 standard at room temperature. The specimen dimensions were 12.68 mm x 3.12 mm x 127 mm and the span was 51.2 mm (a span-to-depth ratio of 16:1). The testing was completed using the MTS 858 load frame with a 25 kN load cell. The strain rate for testing was 0.01 mm/mm/min (crosshead speed of 1.37 mm/min).

2.11 Izod Impact Testing

Izod impact tests were completed on a Tinius Olsen IT 504 for notched specimens following the ASTM D256 standard at room temperature. The pendulum energy was 2.84 J. The nominal dimensions for the Izod specimens were 3.20 mm x 12.5 mm. The depth under the notch was 10 mm. The ABS specimens were 4mm in thickness, while the ABS-L specimens were 3.20 mm in thickness.

2.12 Nanoindentation

Nanoindentation experiments were performed with a Nanomechanics iMicro nano-indentation device equipped with a Berkovich diamond tip. The elastic modulus and Meyer hardness of pure lignin, VF10, VF35, and neat ABS were measured. The results were measured at penetration depths of 200 nm, 500 nm, and 800 nm. The elastic modulus reported is the average elastic modulus at the depth of 180-200 nm for the 200 nm measurement, 300-500 nm for the 500 nm measurement, and 500-800 nm for the 800 nm measurement.

3. RESULTS AND DISCUSSION

3.1 Thermal Characterization

ABS, deodorized lignin, and an ABS-lignin blend with 25% lignin weight fraction (VF25) were thermally characterized using thermogravimetric analysis (TGA) and differential scanning calorimetry (DSC). TGA was used to evaluate all samples from room temperature to 800°C at a heating rate of 10°C/min under nitrogen gas. Weight loss can be attributed to moisture loss and thermal degradation (Figure 6). Table 5 shows the peak decomposition temperatures for each sample. DSC was used to determine the glass transition temperature (T_g). The T_g indicates the temperature when a material transitions from a hard-glassy state to a viscous-rubbery state.

To deduce the appropriate processing conditions for the VF25 thermoplastic blend, it is useful to examine the glass transition and peak decomposition temperature. As shown in Table 1, lignin has a peak degradation temperature approximately 50°C below ABS.

However, the glass transition temperature of lignin is approximately 40°C higher than ABS. The VF25 thermoplastic has a glass transition and peak decomposition temperature that is similar to neat ABS. Based on this data, we can conclude that the thermal and processing behavior of the VF25 thermoplastic more closely resembles the neat ABS thermoplastic than lignin. Blending the neat ABS with lignin requires temperatures well above 155°C such as 200°C, but lower than 250°C as thermal degradation is initiated at 250°C (Figure 6).

Another study using TGA was done where varying temperatures from 180-230°C were held for 30 minutes to determine the rate of degradation. The temperature range of 180-230°C was chosen because this is the typical melting temperature range for ABS, and Figure 6 shows increased degradation occurs after 250°C. Table 6 shows the time it took for each sample to lose 1% of its original weight at the specified hold temperature. Two different lignin weight fractions were tested along with neat ABS, 10% (VF10) and 35% (VF35).

The TGA degradation study establishes the time it takes for samples to achieve a weight loss of 1% to mimic potential degradation during extrusion. Weight loss of more than 1% indicates that the sample has lost its moisture content, and it has begun its chemical degradation phase. It is desirable to prevent significant lignin weight loss during processing of the ABS-L material as it can affect the mechanical properties of the final thermoplastic. Lignin extrusion is also highly temperature dependent as there is a small processing window between chemical decomposition and flow. Therefore, this study enables us to understand the maximum processing time required for the thermoplastic at various temperatures such that significant lignin degradation does not occur. The TGA degradation study shows that samples containing a higher lignin volume fraction (VF35) degrade faster to reach 1% weight

loss than samples containing a lower lignin volume fraction (VF10). The final weight remaining after 30 minutes decreases as the lignin loading is increased in the ABS-L blend. As the VF35 samples contain a higher amount of oxidized lignin, it is reasonable to expect faster degradation. Based on this, lignin-thermoplastic blends must be processed at less than 220°C to prevent faster degradation.

3.1.1 Glass Transition Temperature

The storage modulus in Table 7 was reported as the maximum value from the initial glassy plateau observed between 25-30°C. The storage modulus increases as the lignin content is increased in the blends (additional plots are included in the Supplementary Materials section in the Appendix). This is due to the reinforcement effect of the higher modulus lignin. The loss modulus also increases as the lignin content is increased. The tan δ value decreases with increasing lignin content. This indicates that the ability of the material to dissipate energy decreases as more lignin is added to the blend. This causes the material to have a lesser ability to absorb impact, which is confirmed by Izod impact results (Table 10). A broadening of the tan δ peak was also observed (Figure 14), especially between neat ABS and VF35 peaks. Increasing the lignin content causes the blends to have a wider range of polymer chain lengths. Although lignin is not miscible with ABS resin, it can still form a hydrogen bond with the nitrile group in ABS (Song et al. 2012). This results in a wider distribution of effective polymer lengths, causing the observed broadening of the tan δ peaks.

Table 7 also shows the T_g results obtained using DSC. There is only a 2°C difference in T_g between the neat ABS sample and the VF35 blend. The similar T_g's for all the samples

suggests that there are multiple phases in the blend. In this case, the observed T_g is the T_g for the neat ABS phase of the blend, as the T_g for the lignin is higher.

The glass transition temperature of the blends was lower compared to the neat ABS resin. As this is an immiscible system, the observed T_g is the glass transition of the ABS resin. Akato et al. reported that the incorporation of lignin in ABS lowers the activation energy for the relaxation of hard and soft phases in the material (Akato et al. 2015), which explains the overall decrease in T_g for the blends. The low interfacial compatibility is likely creating additional free volume at the ends of polymer chains, which leads to increased chain mobility, resulting in a lower glass transition temperature. The slight increase in T_g of VF35 compared to VF10 (from E'' peak) may be due to the hindrance of polymer chain movement caused by the increased lignin content (Song et al. 2012), which is a large three-dimensional polymeric molecule.

3.2 Mechanical Properties

3.2.1 Tensile Properties

Tensile testing was completed to show the effects of lignin incorporation into ABS resin. Table 8 shows the tensile properties for neat ABS and ABS-L blends with increasing lignin weight fractions up to 35%. The ABS-L blends show improved tensile modulus compared to neat ABS. The increase in modulus due to lignin incorporation in thermoplastic materials is commonly reported in literature (Pucciariello et al. 2004b; Sahoo et al. 2011; Song et al. 2012). The increase in modulus is a result of the addition of lignin, which has a higher stiffness than the ABS resin, resulting in an overall higher stiffness of the material with increasing lignin content. It is also notable that there is a strong linear trend ($R^2 = 0.9779$) in

tensile modulus with increasing lignin loading (Fig. 8). This linear trend, along with the significant decline in the ultimate strain, indicates that lignin dominates the tensile failure in the blends. The largest increase in tensile modulus occurs when going from neat ABS to VF10, which is also the largest decrease in ultimate strain. This shows the immediate impact on mechanical properties upon lignin addition. When lignin is added to neat ABS, it undergoes the applied tensile stress first, not the neat ABS. The tensile strength is also increased with lignin addition compared to neat ABS. This result did not match our hypothesis that addition of lignin will cause a decrease in tensile strength, which was the general trend observed in literature (Alexy et al. n.d.; Pucciariello et al. 2004b; Sahoo et al. 2011; Song et al. 2012). Overall, the tensile strength increased compared to neat ABS. However, as expected, the tensile strength decreased with increasing lignin loading. Although ABS has a polar -CN group in its polymer chain, polar lignin has poor compatibility with ABS resin, which is largely nonpolar. Increasing lignin content decreases the compatibility between ABS and lignin, causing a decrease in tensile strength due to poor stress transfer from ABS to lignin. The elongation at break decreases with increasing lignin content. This is due to the increasing content of brittle lignin, which reduces the plasticity of ABS resin. Overall, the results indicate that there is poor interfacial adhesion between lignin and ABS. Strong interfacial adhesion would more strongly manifest itself in strength than in stiffness. Stiffness is a bulk property that is more dependent on the volume of the filler, but strength is more strongly affected by the load sharing and transfer between the filler and the matrix.

A maximum strength is achieved at a lignin weight fraction of 10% and 15%. This means that for a maximum strength blend, either 10% or 15% lignin weight fraction can be used. Analysis of variance (ANOVA) was completed for the means of all blends on JMP software. Post-hoc analysis for all mean pairs was completed with Tukey's HSD test on JMP. For tensile strength, the Tukey HSD test confirmed that the means for 10% and 15% blends are not significant (additional information and figures are included in the Supplementary Materials section in the Appendix). Additionally, the connecting letters report for the Tukey HSD test shows that the tensile strength for 20% blend is also not significant relative to the 10% and 15% blends. The results confirmed that there is no statistically significant difference in means for tensile strength for the three blends, but there is a difference in means for tensile modulus and ultimate strain for the same blends (Figures 15 and 16). At 10%, the ultimate strain is higher than at 15%. The tensile modulus at 10% is lower than at 15%. If the application requires a more plastic material, a 10% blend is preferable; for an application that requires a stiffer material, a 15% blend is preferable.

When not accounting for the neat ABS results, it is observed that all tensile properties for the various blends show a strong linear trend. The R^2 values are 0.9819, 0.9291, and 0.9808 for tensile modulus, strength, and ultimate strain, respectively, as shown in Figure 8.

3.2.2 Flexural Analysis

Table 9 shows the flexural properties for neat ABS and ABS-L blends with increasing lignin weight fractions up to 35%. The ABS-L blends show improved flexural modulus compared to neat ABS. The lignin increases the stiffness of the ABS-L blend, increasing the modulus of the material. The flexural strength also increases compared to neat ABS. The flexural

strength remains steady for all blends. Surprisingly, there is no consistent trend of increase or decrease in flexural strength as the lignin content is increased. A study by Song et al. showed an increase in flexural strength with increasing lignin loading (Song et al. 2012). The ultimate strain decreased after the addition of lignin. With increasing lignin content, the ultimate strain continues to decrease as the material becomes more brittle and the compatibility between ABS and lignin decreases.

Based on ANOVA, it was concluded that the means for flexural strength for all ABS-L blends are statistically significant ($p<0.05$). Post-hoc analysis for all mean pairs was completed with Tukey's HSD test. The connecting letters report for means of all pairs indicates that there is no statistically significant difference in means for VF10, VF15, VF20, VF25, and VF30 (Fig. S8). From this, it is concluded that flexural strength of VF35 is a statistically significant mean relative to results for all other blends. However, the connecting letters report also shows that VF35 is not statistically different from VF10 and VF15. The decrease in flexural strength at VF35 can be attributed to the decreasing compatibility of lignin in ABS at a higher lignin loading as lignin-lignin interactions become more prevalent. Based on this analysis, there is no single blend that can be considered to have maximum strength. As such, a blend must be selected in accordance with the flexural modulus and plasticity desired for the application.

Statistical analysis also shows that the means for flexural modulus and ultimate strain for pairs VF10/VF15 and VF15/VF20 are not statistically significant (Fig. S7 and S9). This indicates that, at a lower lignin loading, there is little change in flexural properties of ABS-L. The increased change in properties at higher lignin loadings are likely due to the lack of

interaction between lignin and ABS phases and introduction of more inhomogeneities in the blends due to lignin-lignin polar interactions. For flexural modulus, the means for VF30/VF35 are also not statistically significant.

When not accounting for the neat ABS results, it is observed that flexural modulus and ultimate strain for the various blends show a strong linear trend. The R^2 values are 0.9351 and 0.9623 for flexural modulus and ultimate strain, respectively (Fig. 9).

3.2.3 Izod Impact Resistance

Table 10 shows the impact strength for neat ABS and ABS-L blends with increasing lignin weight fractions up to 35%. The incorporation of lignin decreases the impact resistance of the ABS-L blend compared to neat ABS. All neat ABS specimens had a hinge failure. Approximately one-quarter of the VF10 samples also had a hinge failure, while the remaining VF10 specimens failed with a complete break. The large decrease in impact resistance from neat ABS to VF10 indicates lignin's immediate impact on impact properties, just as it was observed for tensile and flexural properties. For VF10, it can be concluded that the lignin phase dominates the failure behavior. However, the hinge failures for VF10 also suggest that there is some stress transfer from the lignin phase to the ABS phase. All samples with a lignin loading >10% failed with a complete break. As the material became more brittle, a complete break was observed. Therefore, as lignin is a brittle material, the impact resistance continues to decrease as the lignin content is increased. It was discussed above that the tan δ value of the material decreases with increasing lignin content (Table 7). The decreasing tan δ value indicates that the material has lesser ability to dissipate impact energy. Therefore, the Izod impact results agree with the DMA results discussed above. The trend in

impact resistance for the blends resembles an exponential decay function. Using an exponential trendline, an R^2 value of 0.9863 was obtained (Fig. 10). The data shows asymptotic behavior for blends of 30% and 35% lignin. This is also confirmed by Tukey HSD test, which shows that the means for VF30 and VF35 are not significant. It can be concluded that at a lignin loading of 30% and higher, the brittleness of the lignin completely dominates the failure. The ability to dissipate energy from the lignin to the ABS phase has decreased drastically, which is indicated by the decreasing tan δ value (Table 3). This is likely due to the increased lignin-lignin polar interactions in the blends, resulting in the agglomeration of lignin particles. Hence, the formation of lignin particles leads to the lignin dominated brittle failure of VF30 and VF35.

3.3 Optical Microscopy

The two separate phases of the ABS resin are apparent from the optical microscopy images (Fig. 11). The continuous matrix phase is the styrene-acrylonitrile (SAN) phase, and the dispersed phase is the polybutadiene rubber phase (Xu et al. 2005). As shown in Fig. 11, the neat ABS resin has a homogenous SAN phase. After the addition of 10% lignin, the amount and average size of the polybutadiene particles decreases, and the SAN phase is less homogeneous. After the addition of 35% lignin, the average size of the polybutadiene particles increases compared to 10% lignin. The SAN phase is less homogenous compared to neat ABS. Also, there is another discernible phase that appears in VF35 in the form of light gray “particles”, which is likely lignin. The appearance of the third phase indicates the immiscibility of lignin in ABS. The formation of lignin particles can be explained by the strong hydrogen bonding with other lignin molecules. The hydrogen bond between the N in

ABS and H in lignin is weaker compared to the hydrogen bond between O and H on lignin molecules due to the higher difference in electronegativities between O and H, leading to agglomeration of small lignin particles.

After addition of 10% lignin, the size of the polybutadiene rubber particles decreases and remains well-dispersed in the SAN matrix. Lignin is expected to have some nonpolar interactions in the form of van der Waals forces with the hydrocarbon chains in the polybutadiene rubber phase. Addition of 10% lignin enables these non-polar interactions, resulting in the smaller and more homogeneously dispersed rubber particles observed in Figure 11b.

The VF35 blend seems to be more inhomogeneous as compared to VF10. This can be explained by considering the multiple chemical interactions occurring between the SAN and polybutadiene phases with lignin. There is a non-polar interaction between lignin and the hydrocarbon chains in polybutadiene. There is a polar interaction between lignin and acrylonitrile in the SAN matrix. There is also a non-polar interaction between lignin and styrene in the SAN matrix. The polar interaction between lignin and acrylonitrile in the SAN matrix is stronger than the non-polar interaction between lignin and hydrocarbon chains in polybutadiene phase. As a result, lignin interacts more with the SAN matrix than with the polybutadiene rubber phase. This results in the higher average polybutadiene particle size in VF35 compared to VF10 as shown in Table 11 (additional information is included in the Supplementary Materials section in the Appendix). There is also appearance of a light gray phase in VF35 (Fig. 11c), which may be predominantly composed of lignin. A higher lignin content increases the likelihood of lignin-lignin polar interactions in the form of hydrogen

bonds. The SAN phase in VF35 appears less homogeneous than the SAN phase in neat ABS. This is likely a result of competing chemical interactions. Lignin can have a non-polar interaction with the styrene component of SAN and a polar interaction with the acrylonitrile component of SAN. Thus, it can be concluded that at a higher lignin content, the system becomes less miscible/more inhomogeneous due to the agglomeration of lignin particles. Therefore, lignin tends to act like a filler in ABS resin at higher concentrations.

3.4 Nanoindentation

Nanoindentation testing was completed on ABS, VF10, VF35, and 100% lignin fibers. The modulus of the lignin fibers could not be measured via tensile testing as the fibers were too fragile to handle, which made nanoindentation a more suitable method. After they were spun, the lignin fibers were not subjected to any thermal treatment. The elastic modulus was measured at depths of 200 nm, 500 nm, and 800 nm, as shown in Figure 12. The elastic modulus reported is the average elastic modulus at the depth of 180-200 nm for the 200 nm measurement, 300-500 nm for the 500 nm measurement, and 500-800 nm for the 800 nm measurement. The modulus shows a strong dependence on lignin content. There was higher variability in elastic modulus results for VF35 compared to VF10. This is likely due to the lack of miscibility of ABS and lignin and the increased inhomogeneity of the VF35 ABS-L blend.

Neat ABS resin shows similar modulus results as VF10. This indicates that at small lignin loadings, the material properties do not get affected significantly at the microscale. This must be distinguished from the significant change in mechanical properties going from neat ABS to VF10 for the tensile, flexural, and Izod impact tests performed, which measure bulk

properties of the material. Similar coefficients of variation also indicate that blending 10% lignin in ABS has little to no effect on the microstructure of the material. Both ABS and VF10 have a similar range of values for measurements at all depths, indicating the more homogeneous nature of the VF10 blend. VF35 blend has a higher range of values for indentations at all depths, indicating the stronger phase separation in the blend. The minimum moduli of the VF35 blends are similar to the minimum moduli of both ABS and VF10. These minima are the values from the indents on the ABS phase of the blends. The higher maxima values for VF35 are likely caused by indentation measurements on the lignin particles.

A simple rule of mixtures was applied to estimate the nanoindentation modulus of VF10 and VF35 blends. Lignin fibers were used to obtain the nanoindentation modulus of pure lignin. The results are shown in Figure 12. Overall, the estimated values from the rule of mixtures match very well with the measured data. The estimated ROM values fall within one standard deviation of the measured moduli of the samples at all depths (Figure 13). The VF35 modulus at a depth of 500nm is the only significant outlier. Along with the linear trends observed for the tensile and flexural data (Figs. 8 and 9), we can conclude that, if given the properties of neat ABS and pure lignin, we can successfully employ the rule of mixtures to predict the material properties of ABS-L blends, both for bulk properties and properties at the microscale.

4. CONCLUSION

ABS and a novel deodorized Kraft lignin blends were combined via a melt-blending technique and manufactured into test specimens via injection molding. The various blends

were characterized for thermal and mechanical properties. The storage modulus increased with increasing lignin loading due to the reinforcing effect from the higher modulus lignin. The tan δ value decreased with increasing lignin loading, indicating the material's decreased ability to dissipate energy upon impact. This was confirmed by the decreasing impact resistance of the material with increasing lignin loading. Both the tensile and flexural moduli increased upon lignin addition due to lignin's reinforcing effect. However, the ultimate strain for both the tensile and flexural tests decreased as the lignin loading increased, indicating that the material transitions from ductile failure to brittle failure. Linear trends were observed for both tensile and flexural moduli as well as the ultimate strain for both tests. This indicates that lignin dominates the failure of the blends. Optical microscopy images show the agglomeration of lignin particles in VF35, which shows that poor miscibility between lignin and ABS. The lignin particles cause increasingly brittle failures in blends with higher lignin loadings. The nanoindentation elastic modulus showed a strong dependence on lignin content. The elastic modulus was similar for ABS and VF10 at the microscale, indicating that lower lignin loadings do not show an impact on the blend's microstructure. Using the rule of mixtures, it was discovered that the material properties of ABS-L blends can be predicted quite accurately at the microscale.

Based on the results of this study, it can be concluded that lignin tends to act as a filler in ABS. Addition of deodorized lignin to ABS enhances mechanical properties such as tensile modulus and strength as well as flexural modulus and strength. It is best to formulate ABS-L blends with a lower lignin fraction for commercial applications. Increasing the lignin loading causes the blend to transition from being a more ductile material to a much more brittle

material with very little ability to absorb impact, decreasing material properties such as ultimate strain and impact resistance. Overall, this study establishes the viability of using deodorized lignin for use in commercial applications in the form of thermoplastic composites.

REFERENCES

[1] Boerjan W, Ralph J, Baucher M. Lignin Biosynthesis. Annu Rev Plant Biol 2003;54:519–46. https://doi.org/10.1146/annurev.arplant.54.031902.134938.

[2] The next generation LignoBoost-tailor-maid lignin production for different lignin bioproduct markets. 2017.

[3] Mai C, Milstein O, Hü A. Chemoenzymatical grafting of acrylamide onto lignin. vol. 79. 2000.

[4] Marquardt W, Harwardt A, Hechinger M, Kraemer K, Viell J, Voll A. The biorenewables opportunity - toward next generation process and product systems. AIChE Journal 2010;56. https://doi.org/10.1002/aic.12380.

[5] Tran H, Vakkilainnen EK. The Kraft Chemical Recovery Process. TAPPI Kraft Recovery Course 2012.

[6] Wang C, Kelley SS, Venditti RA. Lignin-Based Thermoplastic Materials. ChemSusChem 2016;9. https://doi.org/10.1002/cssc.201501531.

[7] Ragauskas AJ, Beckham GT, Biddy MJ, Chandra R, Chen F, Davis MF, et al. Lignin valorization: Improving lignin processing in the biorefinery. Science (1979) 2014;344. https://doi.org/10.1126/science.1246843.

[8] Bajwa DS, Pourhashem G, Ullah AH, Bajwa SG. A concise review of current lignin production, applications, products and their environment impact. Ind Crops Prod 2019;139. https://doi.org/10.1016/j.indcrop.2019.111526.

[9] Mandlekar N, Cayla A, Rault F, Giraud S, Salaün F, Malucelli G, et al. An Overview on the Use of Lignin and Its Derivatives in Fire Retardant Polymer Systems. Lignin - Trends and Applications, InTech; 2018. https://doi.org/10.5772/intechopen.72963.

[10] Lu X, Gu X. A review on lignin pyrolysis: pyrolytic behavior, mechanism, and relevant upgrading for improving process efficiency. Biotechnology for Biofuels and Bioproducts 2022;15. https://doi.org/10.1186/s13068-022-02203-0.

[11] Parit M, Jiang Z. Towards lignin derived thermoplastic polymers. Int J Biol Macromol 2020;165:3180–97. https://doi.org/10.1016/j.ijbiomac.2020.09.173.

[12] Song P, Cao Z, Meng Q, Fu S, Fang Z, Wu Q, et al. Effect of lignin incorporation and reactive compatibilization on the morphological, rheological, and mechanical properties of ABS resin. Journal of Macromolecular Science, Part B: Physics 2012;51:720–35. https://doi.org/10.1080/00222348.2011.609794.

[13] Kadla JF, Kubo S. Lignin-based polymer blends: Analysis of intermolecular interactions in lignin-synthetic polymer blends. Compos Part A Appl Sci Manuf, vol. 35, 2004, p. 395–400. https://doi.org/10.1016/j.compositesa.2003.09.019.

[14] Li Y, Mlyna´r J, Mlyna´r M, Sarkanen S. The First 85% Kraft Lignin-Based Thermoplastics*. vol. 35. John Wiley & Sons, Inc; 1997.

[15] Pucciariello R, Villani V, Bonini C, D'Auria M, Vetere T. Physical properties of straw lignin-based polymer blends. Polymer (Guildf) 2004;45:4159–69. https://doi.org/10.1016/j.polymer.2004.03.098.

[16] Akato K, Tran CD, Chen J, Naskar AK. Poly(ethylene oxide)-Assisted Macromolecular Self-Assembly of Lignin in ABS Matrix for Sustainable Composite Applications. ACS Sustain Chem Eng 2015;3:3070–6. https://doi.org/10.1021/acssuschemeng.5b00509.

[17] Thielemans W, Wool RP. Lignin esters for use in unsaturated thermosets: Lignin modification and solubility modeling. Biomacromolecules 2005;6:1895–905. https://doi.org/10.1021/bm0500345.

[18] Kim Y, Suhr J, Seo HW, Sun H, Kim S, Park IK, et al. All Biomass and UV Protective Composite Composed of Compatibilized Lignin and Poly (Lactic-acid). Sci Rep 2017;7. https://doi.org/10.1038/srep43596.

[19] Nevrez LAM, Casarrubias LB, Celzard A, Fierro V, Mũoz VT, Davila AC, et al. Biopolymer-based nanocomposites: Effect of lignin acetylation in cellulose triacetate films. Sci Technol Adv Mater 2011;12. https://doi.org/10.1088/1468-6996/12/4/045006.

[20] Cachet N, Camy S, Benjelloun-Mlayah B, Condoret JS, Delmas M. Esterification of organosolv lignin under supercritical conditions. Ind Crops Prod 2014;58:287–97. https://doi.org/10.1016/j.indcrop.2014.03.039.

[21] Lisperguer J, Perez P, Urizar S. Structure and Thermal Properties of Lignins: Characterization by Infrared Spectroscopy and Differential Scanning Calorimetry. vol. 54. 2009.

[22] Alexy P, Košíková B, Podstránska G. The effect of blending lignin with polyethylene and polypropylene on physical properties. n.d.

[23] Alexy P, Košíková B, Crkonová G, Gregorová A, Martiš P. Modification of lignin-polyethylene blends with high lignin content using ethylene-vinylacetate copolymer as modifier. J Appl Polym Sci 2004;94:1855–60. https://doi.org/10.1002/app.20716.

[24] González Sánchez C, Expósito Alvarez LA. Micromechanics of lignin/polypropylene composites suitable for industrial applications a. vol. 272. 1999.

[25] Li J, Chua CS. Transductive inference for color-based particle filter tracking. IEEE International Conference on Image Processing, vol. 3, 2003, p. 949–52. https://doi.org/10.1002/pi.1137.

[26] Sahoo S, Misra M, Mohanty AK. Enhanced properties of lignin-based biodegradable polymer composites using injection moulding process. Compos Part A Appl Sci Manuf 2011;42:1710–8. https://doi.org/10.1016/j.compositesa.2011.07.025.

[27] Li - Polyhydroxyalkanoates - opening doors for a sustainable future n.d.

[28] The next generation LignoBoost-tailor-maid lignin production for different lignin bioproduct markets. 2017.

[29] Standard Test Method for Tensile Properties of Plastics 1 n.d. https://doi.org/10.1520/D0638-14.

[30] Standard Test Methods for Flexural Properties of Unreinforced and Reinforced Plastics and Electrical Insulating Materials 1 n.d. https://doi.org/10.1520/D0790-17.

[31] D256 - Izod Impact Testing for Plastics n.d.

[32] Xu XF, Wang R, Tan ZY, Yang HD, Zhang MY, Zhang HX. Effects of polybutadiene-g-SAN impact modifiers on the morphology and mechanical behaviors of ABS blends. Eur Polym J 2005;41:1919–26. https://doi.org/10.1016/j.eurpolymj.2005.02.025.

APPENDIX

TABLES

Table 1: CHNS analysis of all lignin types

	Carbon (%)	Hydrogen (%)	Nitrogen (%)	Sulfur (%)
L1	64.75 ± 0.08	5.95 ± 0.11	0	1.62 ± 0.01
L2	64.42 ± 0.09	5.99 ± 0.03	0	1.88 ± 0.01
L3	63.95 ± 0.11	5.99 ± 0.11	0.12 ± 0.03	2.10 ± 0.01
L4	63.82 ± 0.11	5.76 ± 0.02	0.11 ± 0.01	2.57 ± 0.01

Table 2: Assignment of lignin and their IR bands. (Sammons et al. 2013b)

Observed Band (cm^{-1})	Band Assignment
1515	C-C stretching of aromatic ring
1325	C-O stretching of S ring
1267	C-O stretching of G ring
1212	C-C, C-O, C=O stretch in G ring
1145	C-H stretch in G ring
1139	C-H stretching in G ring
1047	C-O-C stretching of ether groups
915	C-H bending of G units
815	C-H bending of S units

Table 3: P-NMR results (mmol OH/g lignin per sample)

	L1	L2	L3	L4
Aliphatic	1.91	3.31	2.99	1.33
5-Substituted	1.60	2.10	2.71	1.58
Guaiacyl	2.61	3.03	3.75	2.80
p-hydroxyphenyl	0.32	0.77	0.51	0.22
Total Phenolic	4.53	5.90	6.97	4.60
Carboxyl	0.44	0.40	0.60	0.38
Phenolic:Aliphatic	2.37	1.78	2.33	3.46

Table 4: Decomposition temperature, glass transition temperature, and molecular weights of lignin samples.

	Decomposition (°C)	Glass Transition (°C)	M_n	M_w/M_n
L1	401	155.1	2058	2.33
L2	381	148.8	2207	2.30
L3	380	152.2	2037	2.35
L4	380	141.7	1469	1.52

Table 5: Thermal data of ABS, lignin, and VF25. T_g as well as peak decomposition temperature.

Sample	Glass Transition (°C)	Peak Decomposition (°C)	Weight Remaining (%)		
			200 °C	300 °C	800 °C
ABS	112	453	99.8	99.3	2.2
Deodorized Lignin	155	401	97.5	91.8	36
VF25	111	443	99.7	98.2	13.7

Table 6: TGA degradation study. Degradation times of neat ABS and ABS-L blends.

Hold Temperature (°C)	Time to reach 1% weight loss (min)		Final Weight Remaining (%)	
	VF20	VF35	VF20	VF35
180	25.6		98.8	99.1
190	18.1	28.7	98.6	98.8
200	13.9	18.5	98.4	98.5
210	11.7	14.4	98.1	98.1
220	11.1	12.7	97.8	97.6
230	10.8	11.5	97.3	96.8

Table 7: Dynamic mechanical analysis and glass transition temperature data for neat ABS and ABS-L blends.

Sample	Storage Modulus (GPa)	Loss Modulus (GPa)	tanδ	T_g from E'' peak (°C)	T_g from DSC (°C)
ABS	2.32E+09	3.66E+08	1.66	109.3	110.3
VF10	2.48E+09	4.01E+08	1.56	102.3	109.2
VF35	3.38E+09	5.51E+08	1.11	104.4	108.4

Table 8: Tensile test results for neat ABS and ABS-L blends.

Lignin Weight Fraction (%)	Number of Samples (n)	Tensile Modulus (GPa)	Tensile Strength (MPa)	Ultimate Strain (%)
Neat ABS	5	1.58 ± 0.02	29.2 ± 0.84	4.76 ± 0.13
10	21	2.01 ± 0.04	40.6 ± 0.26	2.50 ± 0.06
15	21	2.13 ± 0.05	40.6 ± 0.69	2.36 ± 0.07
20	21	2.21 ± 0.06	39.6 ± 1.16	2.01 ± 0.15
25	21	2.31 ± 0.09	36.8 ± 1.31	1.63 ± 0.06
30	21	2.50 ± 0.06	35.7 ± 1.20	1.45 ± 0.07
35	20	2.64 ± 0.07	33.0 ± 1.26	1.27 ± 0.06

Table 9: Flexural test results for ABS and ABS-L blends.

Lignin Weight Fraction (%)	Number of Samples (n)	Flexural Modulus (GPa)	Flexural Strength (MPa)	Ultimate Strain (%)
Neat ABS	5	1.69 ± 0.11	51.2 ± 1.30	4.66 ± 0.53
10	13	2.66 ± 0.17	69.1 ± 1.69	3.48 ± 0.35
15	7	2.69 ± 0.10	68.4 ± 3.50	3.40 ± 0.35
20	21	2.87 ± 0.17	70.5 ± 2.23	3.23 ± 0.17
25	21	2.87 ± 0.20	69.5 ± 3.59	2.92 ± 0.17
30	21	3.12 ± 0.19	70.5 ± 2.42	2.64 ± 0.12
35	21	3.14 ± 0.15	66.9 ± 2.18	2.30 ± 0.08

Table 10: Izod impact resistance for neat ABS and ABS-L blends.

Lignin Weight Fraction (%)	Number of Samples (n)	Break Energy (J)	Impact Resistance (J/m)
Neat ABS	5	0.582 ± 0.008	145.5 ± 2.09
10	18	0.254 ± 0.017	80.3 ± 5.40
15	21	0.151 ± 0.011	47.5 ± 3.41
20	21	0.089 ± 0.013	27.9 ± 4.06
25	21	0.072 ± 0.006	22.6 ± 1.77
30	21	0.044 ± 0.005	13.8 ± 1.55
35	21	0.037 ± 0.003	11.8 ± 1.05

Table 11: Average size of polybutadiene particles observed in Fig 11.

Sample	Average size (μm^2)
ABS	0.387
VF10	0.110
VF35	0.202

FIGURES

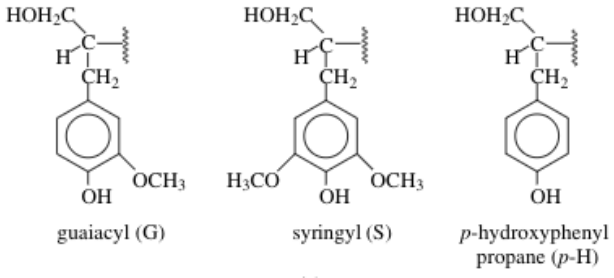


Figure 1: Structural units (monolignols) of lignin (Tejado et al. 2007)

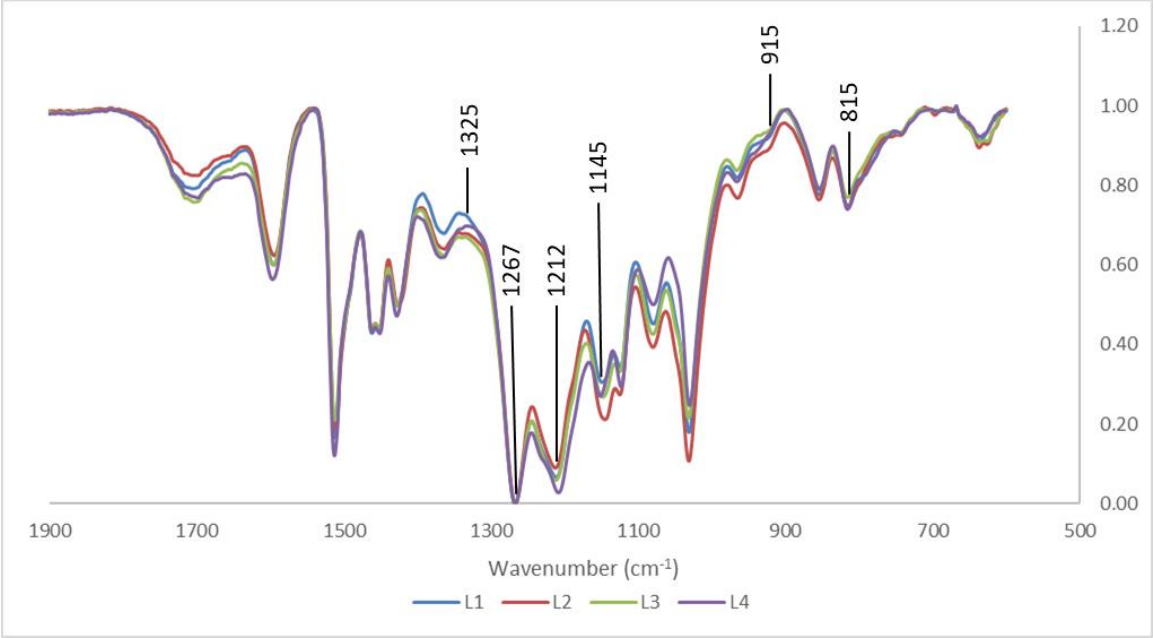


Figure 2: FTIR spectra for all lignin types. L1 and L2 are odor reduced samples while L3 and L4 are not.

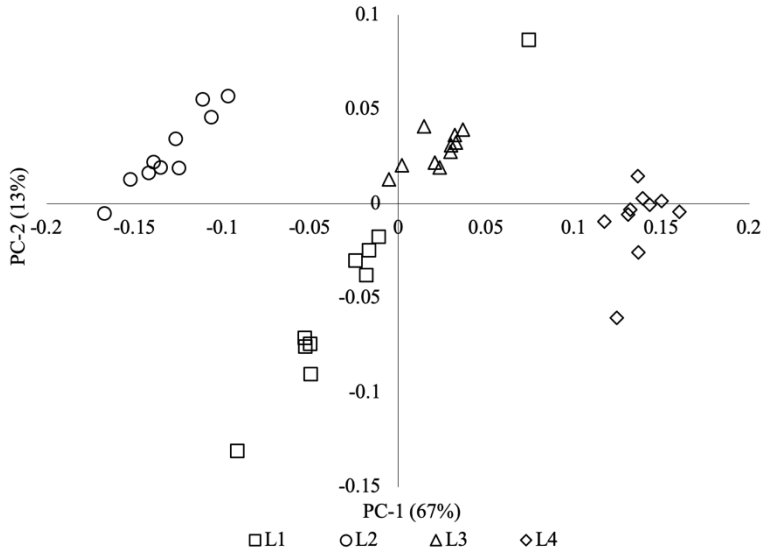


Figure 3: PCA of all lignin types. PC-1 accounts for 67% of the variance among the specimens, while PC-2 accounts for 13% of the variance. Overall, the range of PCs and the difference in grouping is not significant.

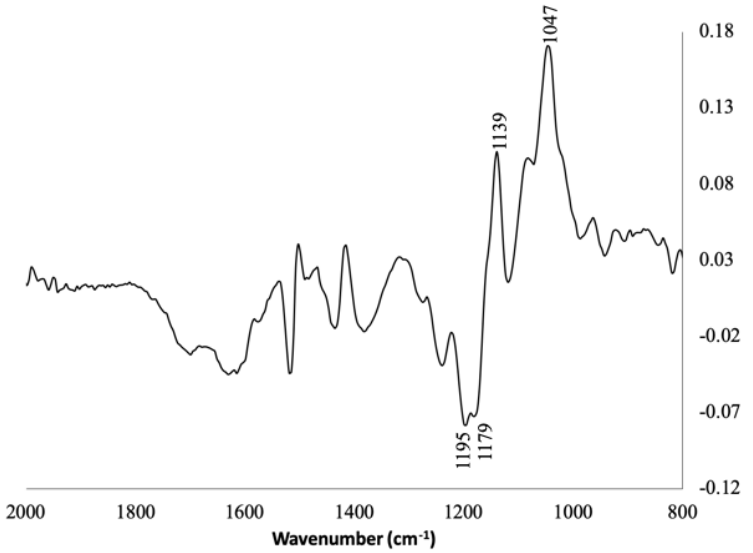


Figure 4: PC-1 loadings

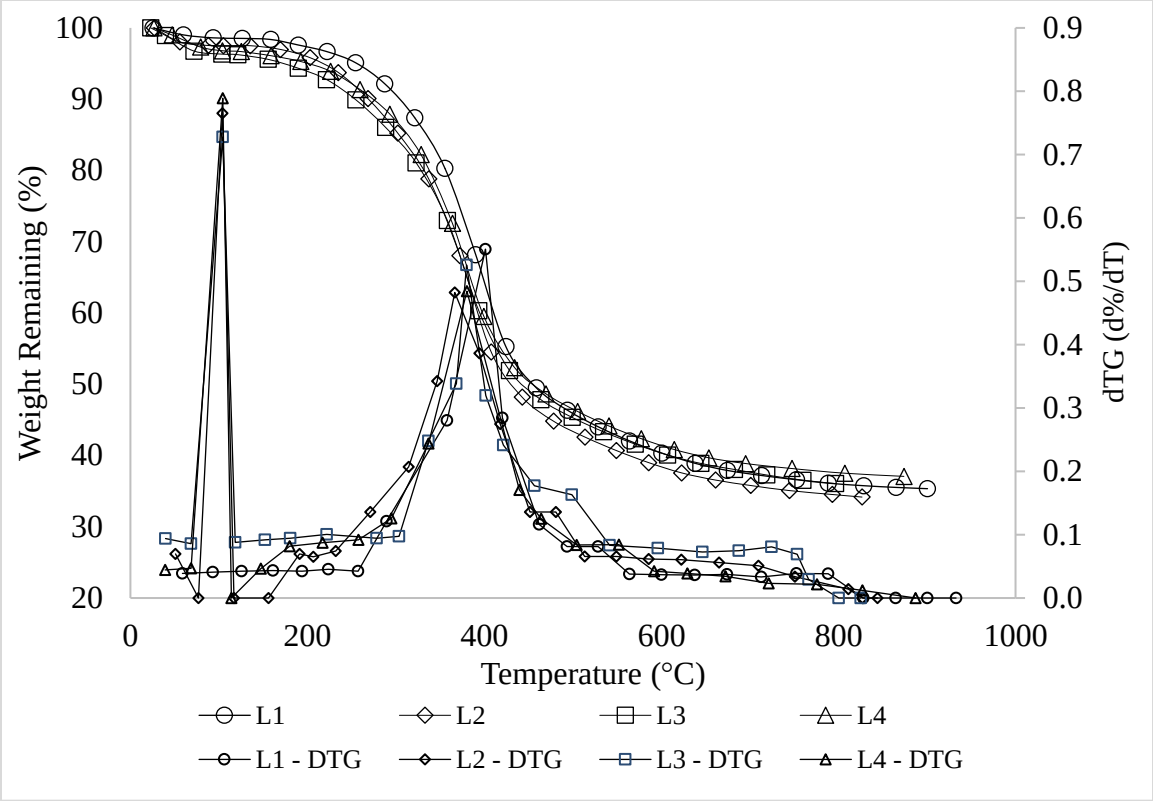


Figure 5: TGA and DTG for all lignin types. L1, the species with the highest decomposition temperature, is obviously shown here while L2, L3, and L4 have very similar decomposition rates and temperatures.

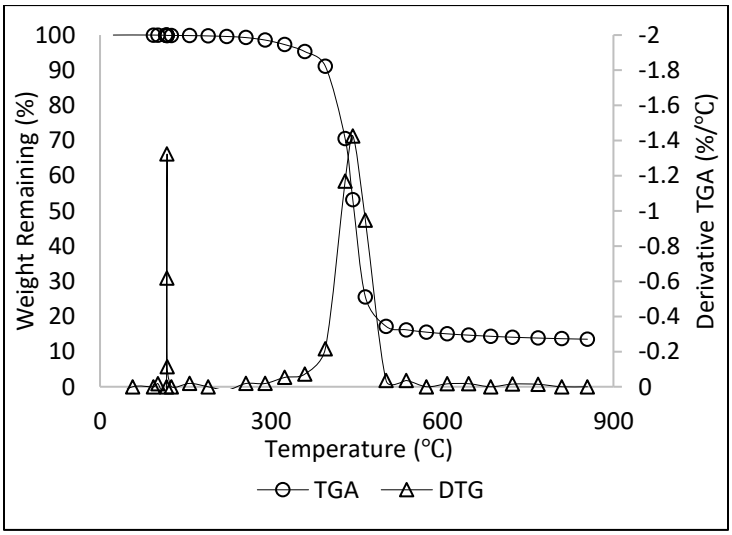


Figure 6: TGA of VF25. The sharp peak just above 100°C is the loss of moisture from the sample.

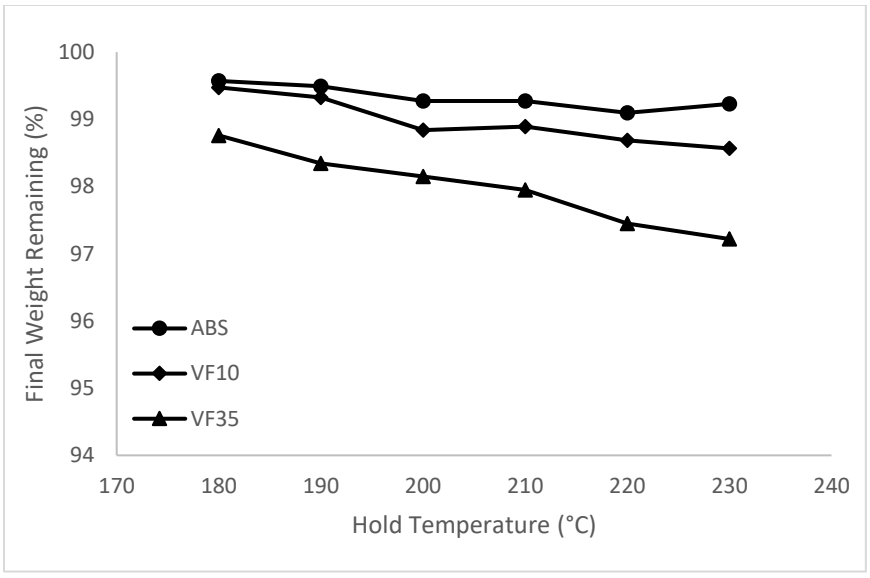


Figure 7: Final weight remaining from TGA degradation study.

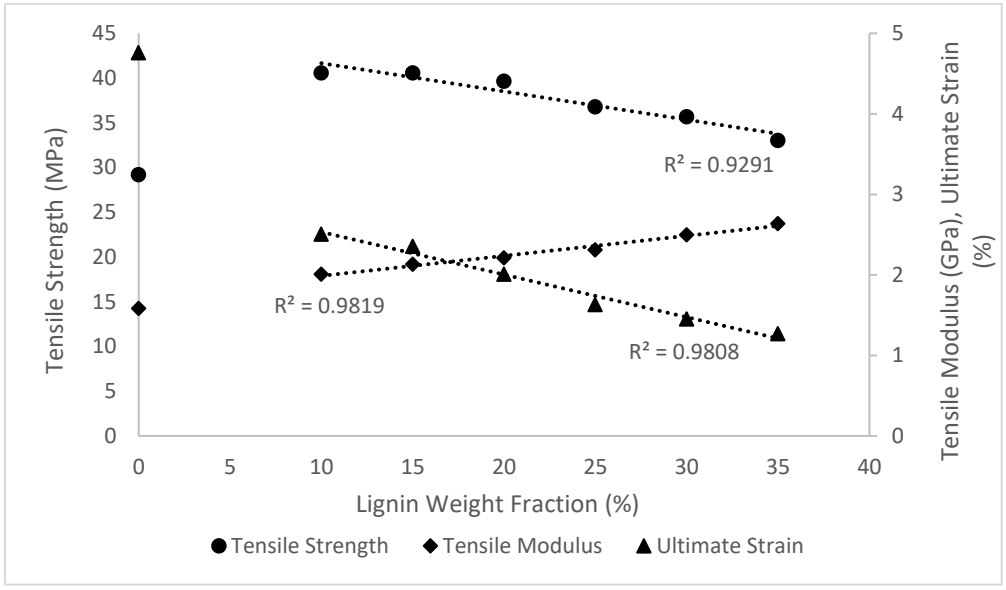


Figure 8: Tensile results of ABS-L blends show strongly linear trends for tensile modulus, strength, and ultimate strain, indicating that the ABS-L blends show a strong correlation of tensile properties with the Rule of Mixtures.

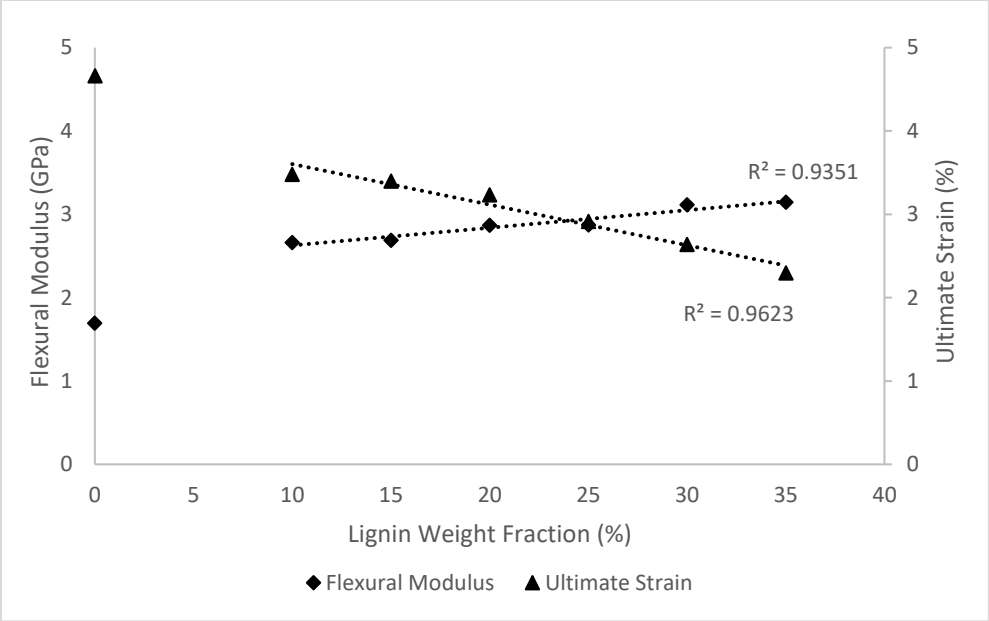


Figure 9: Flexural results of ABS-L blends show strongly linear trends for flexural modulus and ultimate strain, indicating that the ABS-L blends show a strong correlation of flexural properties with the Rule of Mixtures.

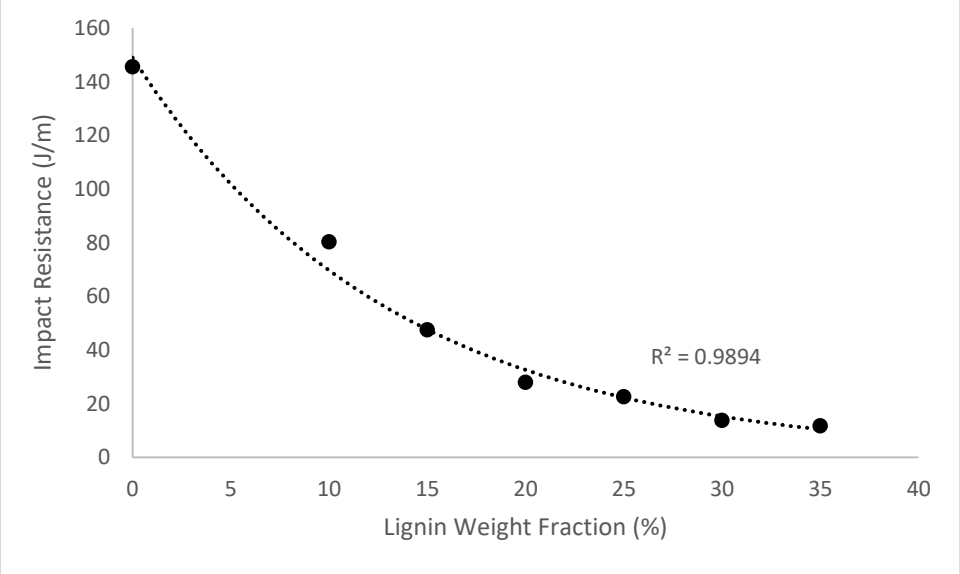


Figure 10: Izod impact results of ABS-L blends show an exponential decay trend for impact resistance.

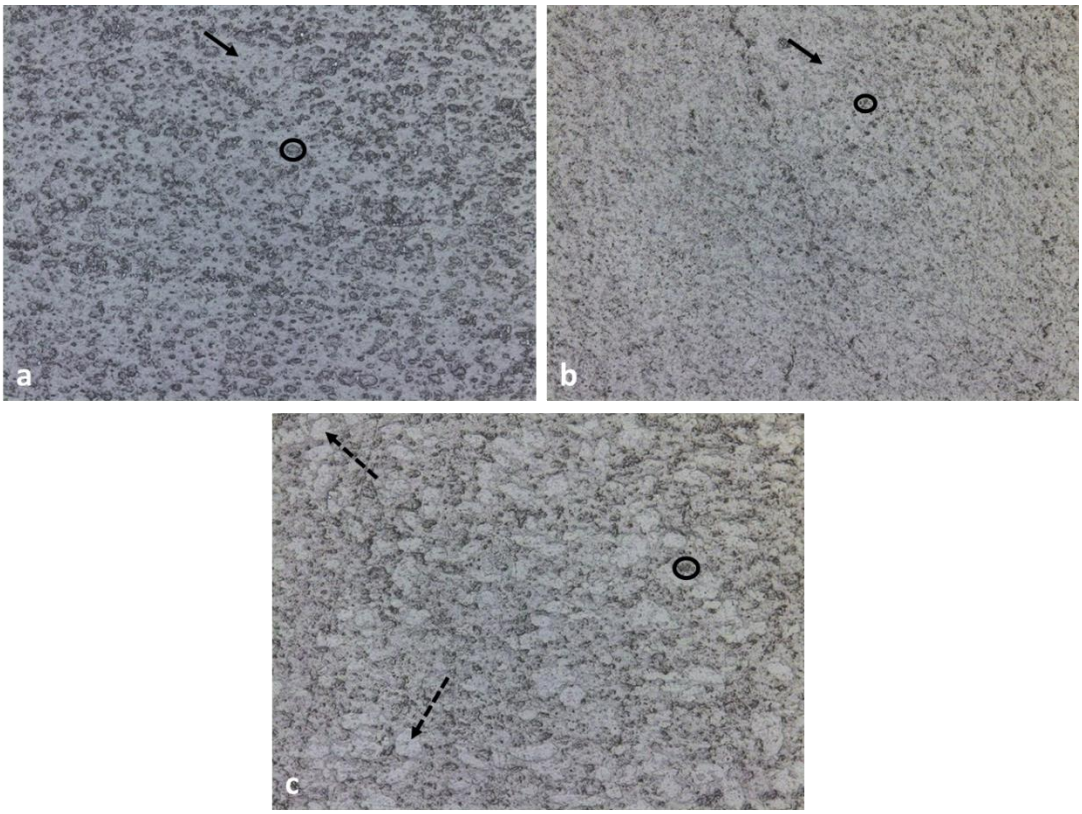


Figure 11: Optical microscopy images for a) neat ABS-1 (left) and neat ABS-2 (right), b) VF10, and c) VF35. The solid arrows point to the continuous SAN phase, the circles indicate the dispersed polybutadiene rubber phase, and the dashed arrows indicate the lignin.

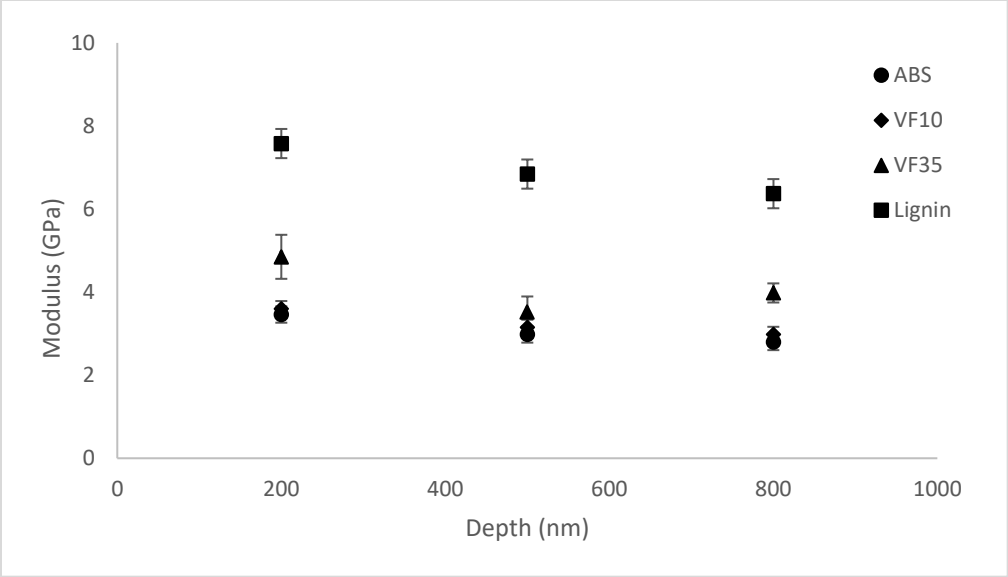


Figure 12: Nanoindentation elastic moduli

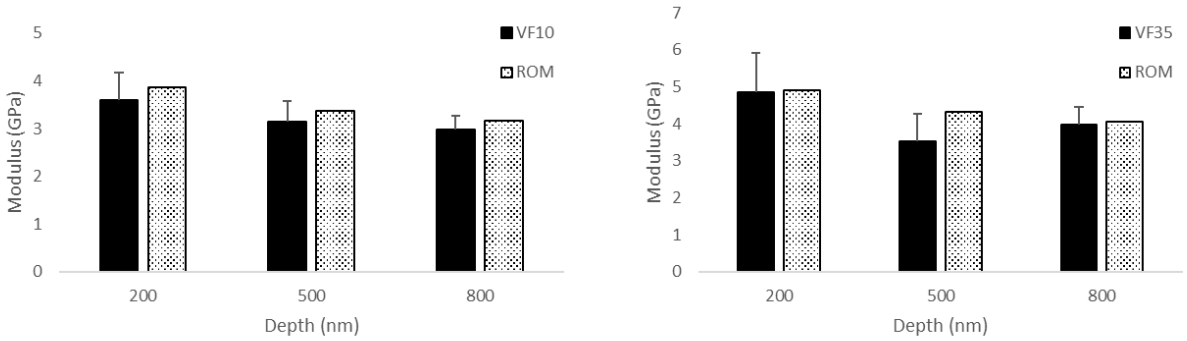


Figure 13: Comparison of measured moduli with simple rule of mixtures (ROM) moduli for VF10 and V35

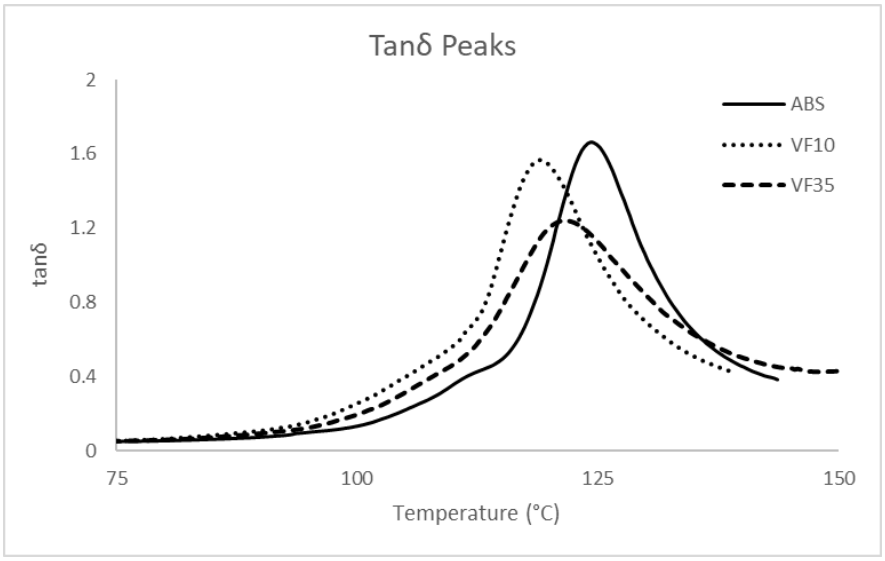


Figure 14: A broadening of the tanδ peaks was observed, indicating the presence of a wider range of polymer chain lengths in VF35 compared to neat ABS.

SUPPLEMENTARY MATERIALS

1. *Dynamic mechanical analysis plots*

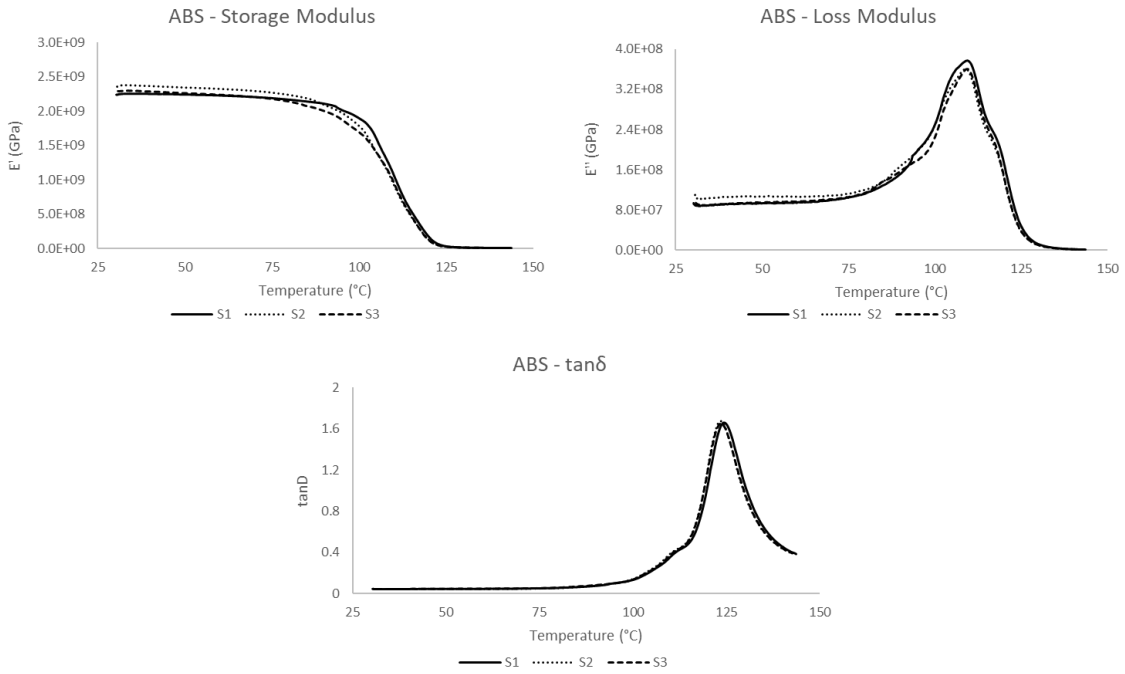


Figure S1: ABS DMA curves

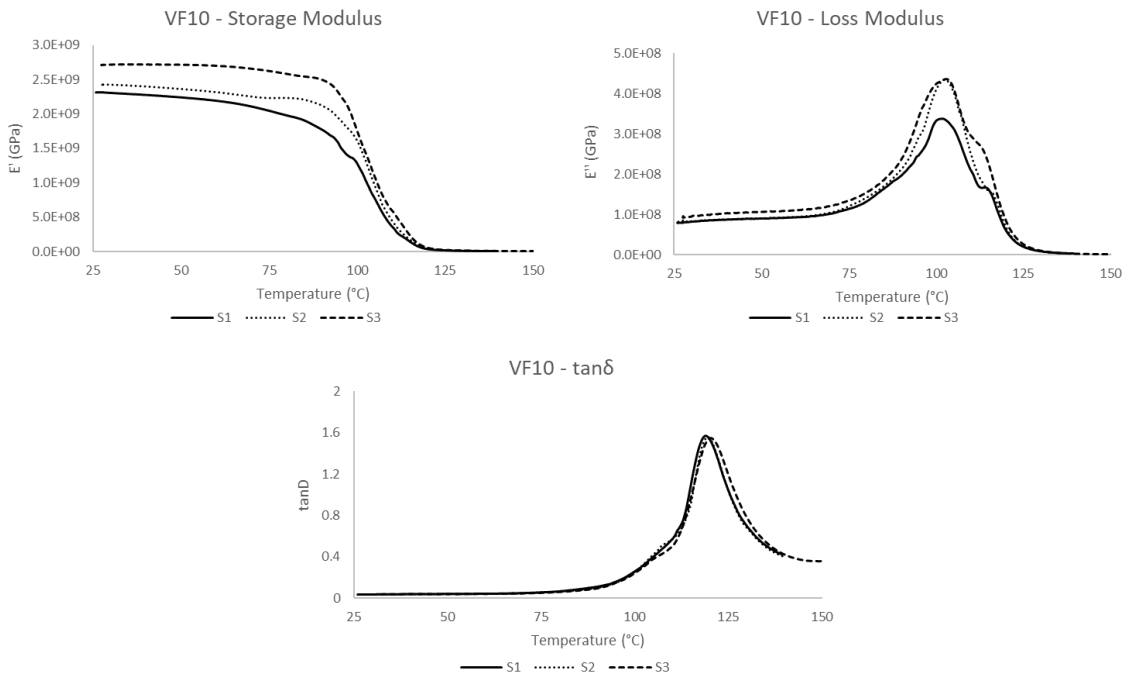


Figure S2: VF10 DMA curves

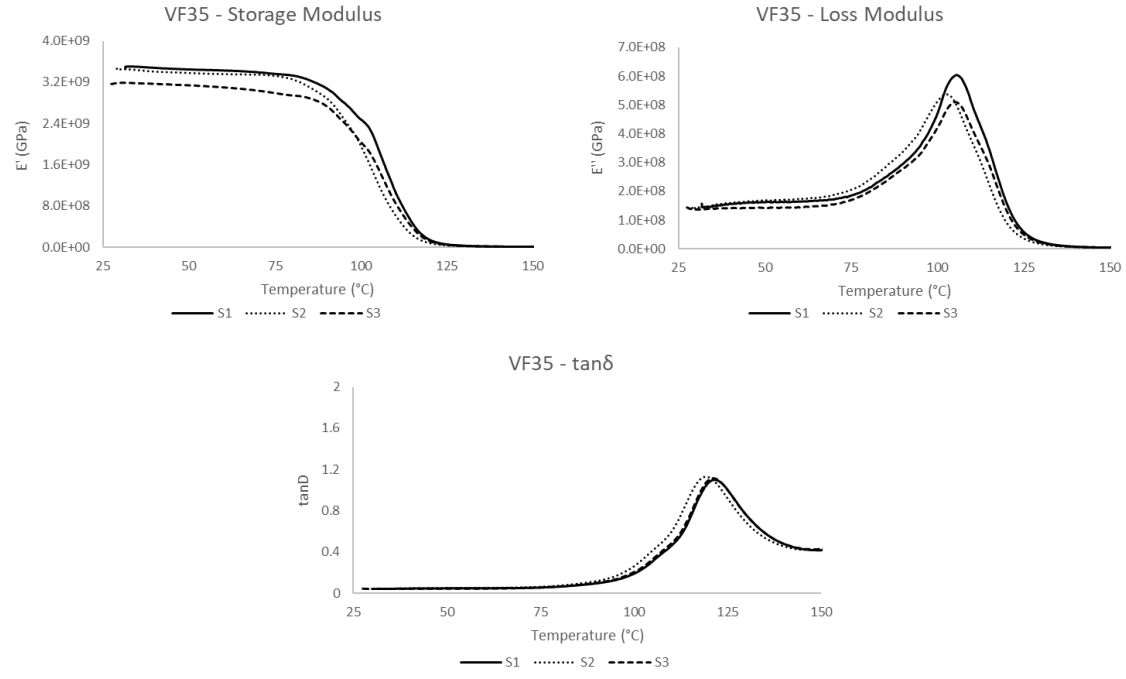
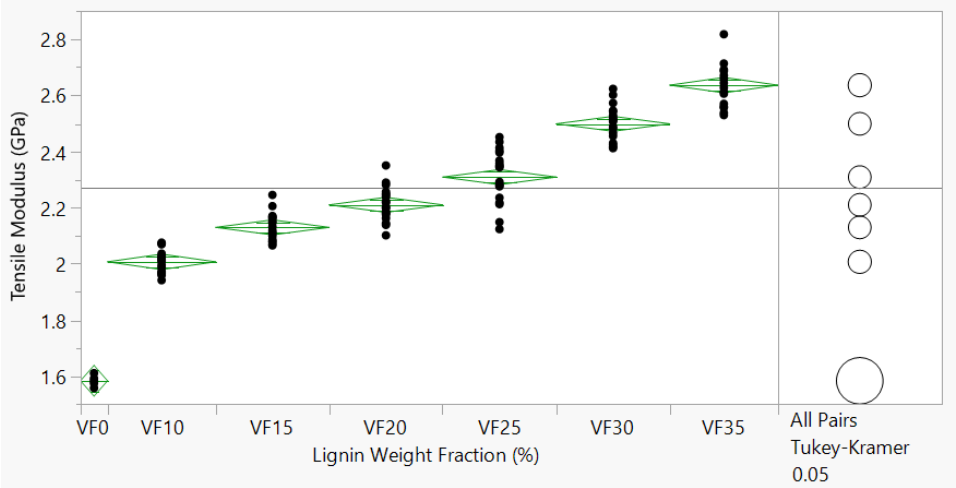


Figure S3: VF35 DMA curves

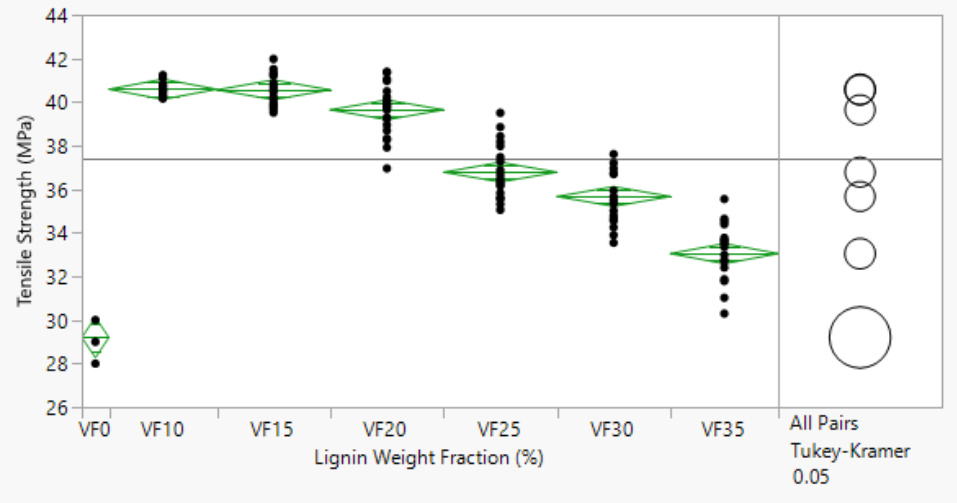
2. Statistical analysis

JMP software was used for the statistical analysis of mechanical data. The data was plotted using the “Fit Y by X” function with the lignin weight fractions being the X factor and the desired mechanical property as the Y response. After the plot is created, the one-way ANOVA option was selected for all mechanical properties to test the means for multiple populations of data points. As the p-value was <0.05 for all one-way ANOVA, we can reject the null hypothesis, which is that all the lignin weight fractions have equal means. As the null hypothesis for the ANOVA was rejected, a post-hoc Tukey-Kramer test was conducted to compare means. The connecting letters report in the figures below shows the results of the Tukey-Kramer test. Samples that are not connected by the same letter are statistically significant.



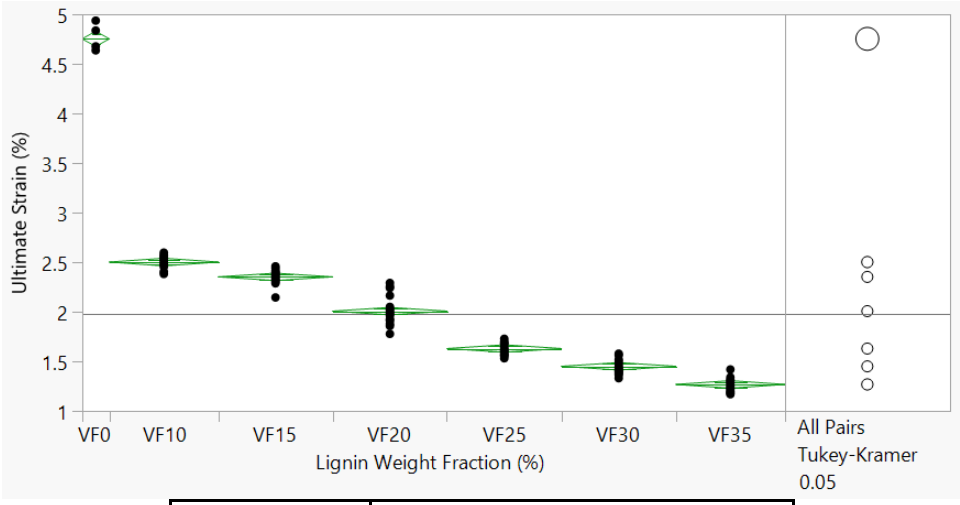
Lignin Weight Fraction (%)	Connecting Letters
Neat ABS	A
10%	B
15%	C
20%	D
25%	E
30%	F
35%	G

Figure S4: Tensile modulus – ANOVA (above) and connecting letters report (below). In the connecting letters report, the Tukey HSD test shows that tensile strength for all blends is statistically significant.



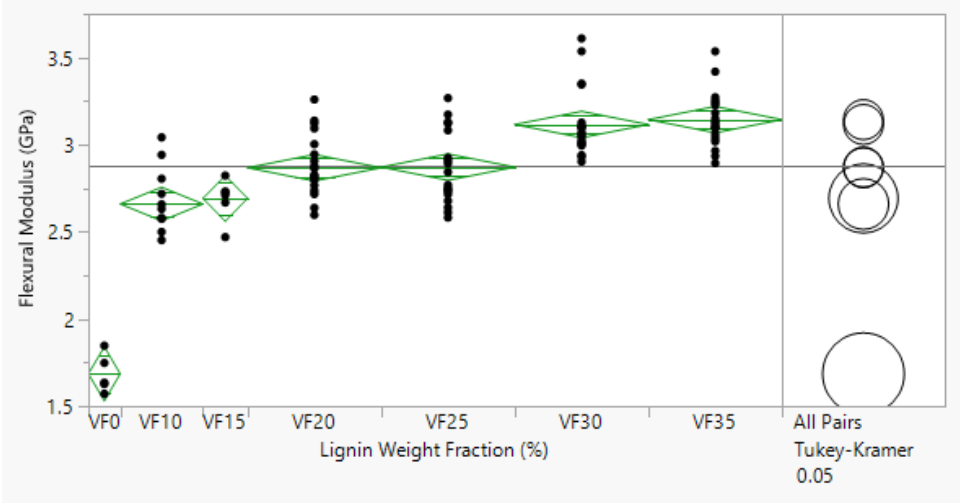
Lignin Weight Fraction (%)	Connecting Letters
Neat ABS	A
10%	B
15%	B
20%	B
25%	C
30%	D
35%	E

Figure S5: Tensile strength – ANOVA (above) and connecting letters report (below). In the connecting letters report, the Tukey HSD test shows that there is no statistical significance in tensile strengths for the 10%/15%/20% blends.



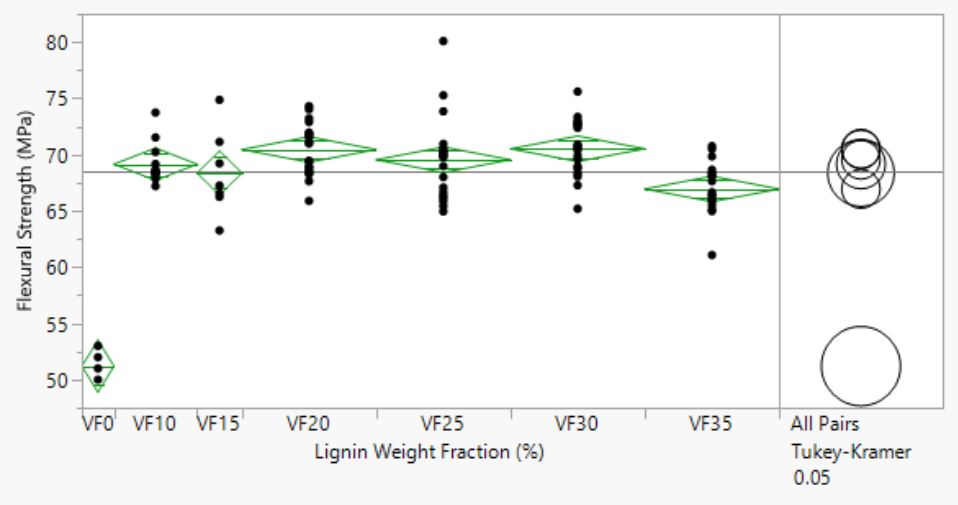
Lignin Weight Fraction (%)	Connecting Letters
Neat ABS	A
10%	B
15%	C
20%	D
25%	E
30%	F
35%	G

Figure S6: Tensile strain at max strength – ANOVA (above) and connecting letters report (below). In the connecting letters report, the Tukey HSD test shows that tensile strain at max strength for all blends is statistically significant.



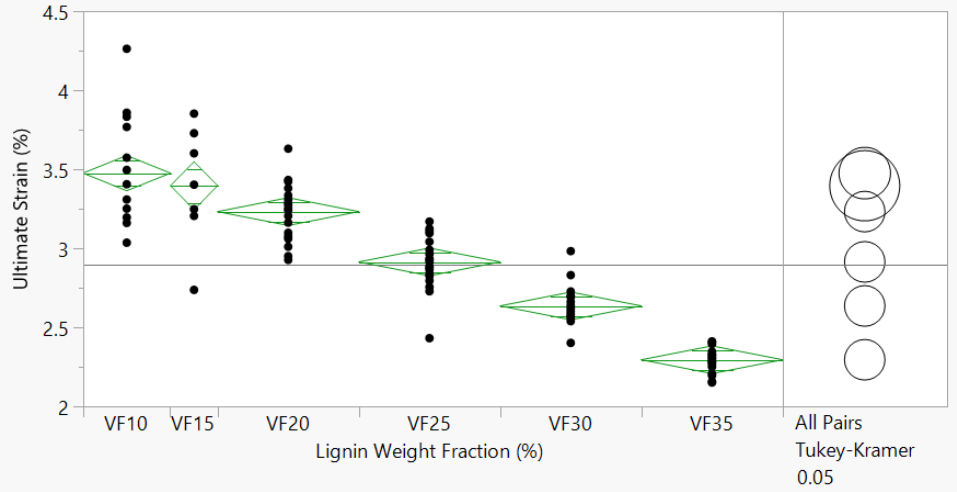
Lignin Weight Fraction (%)	Connecting Letters
Neat ABS	A
10%	B
15%	B C
20%	C
25%	C
30%	D
35%	D

Figure S7: Flexural modulus – ANOVA (above) and connecting letters report (below). In the connecting letters report, the Tukey HSD test shows that there is no statistical significance in flexural modulus for the 10%/15%, 15%/20%/25%, and 30%/35% blends.



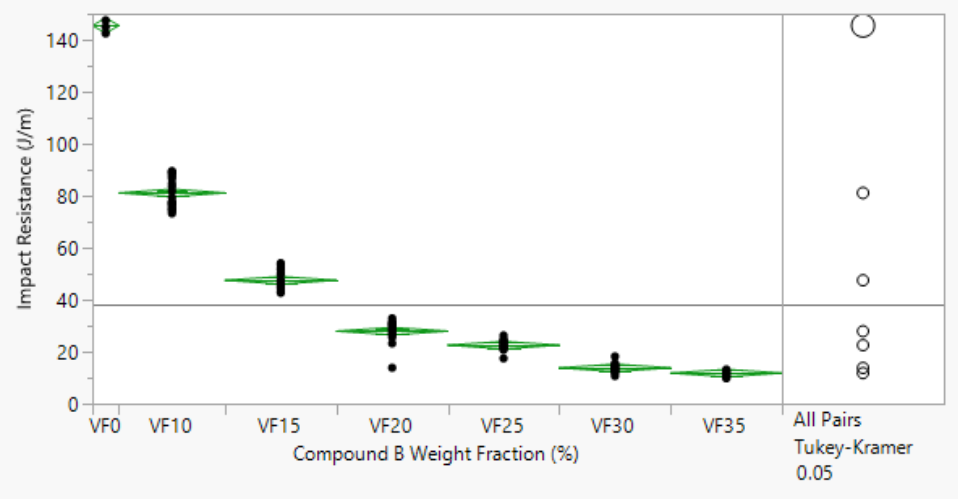
Lignin Weight Fraction (%)	Connecting Letters	
Neat ABS	A	
10%	B	C
15%	B	C
20%	B	
25%	B	
30%	B	
35%		C

Figure S8: Flexural strength – ANOVA (above) and connecting letters report (below). In the connecting letters report, the Tukey HSD test shows that there is no statistical significance in flexural strengths for the 10%/15%/20%/25%/30% and 10%/15%/35% blends.



Lignin Weight Fraction (%)	Connecting Letters
10%	A
15%	A B
20%	B
25%	C
30%	D
35%	E

Figure S9: Flexural strain at max strength – ANOVA (above) and connecting letters report (below). In the connecting letters report, the Tukey HSD test shows that there is no statistical significance in flexural strain at max strength for the 10%/15% and 15%/20% blends.



Lignin Weight Fraction (%)	Connecting Letters
Neat ABS	A
10%	B
15%	C
20%	D
25%	E
30%	F
35%	F

Figure S10: Izod impact resistance – ANOVA (above) and connecting letters report (below). In the connecting letters report, the Tukey HSD test shows that there is no statistical significance in impact resistance for the 30%/35% blends.

3. Image analysis

ImageJ was used for polybutadiene particle analysis from optical microscopy images shown in Figure 6. First, thresholding was completed on each image to turn the image into a binary image as shown in Figure S11. From the binary image, the noise was removed by removing any black particles that were smaller than 0.01-0.02 microns in radius. The radius size for noise removal was determined by visually comparing the binary image to the original image to ensure best representation of the original image. Lastly, the "Analyze Particles" function was used to measure particle radius for all polybutadiene particles in the binary image. In the "Analyze Particles" settings, particles with size >0 microns and a circularity of 0-1 were selected for analysis.

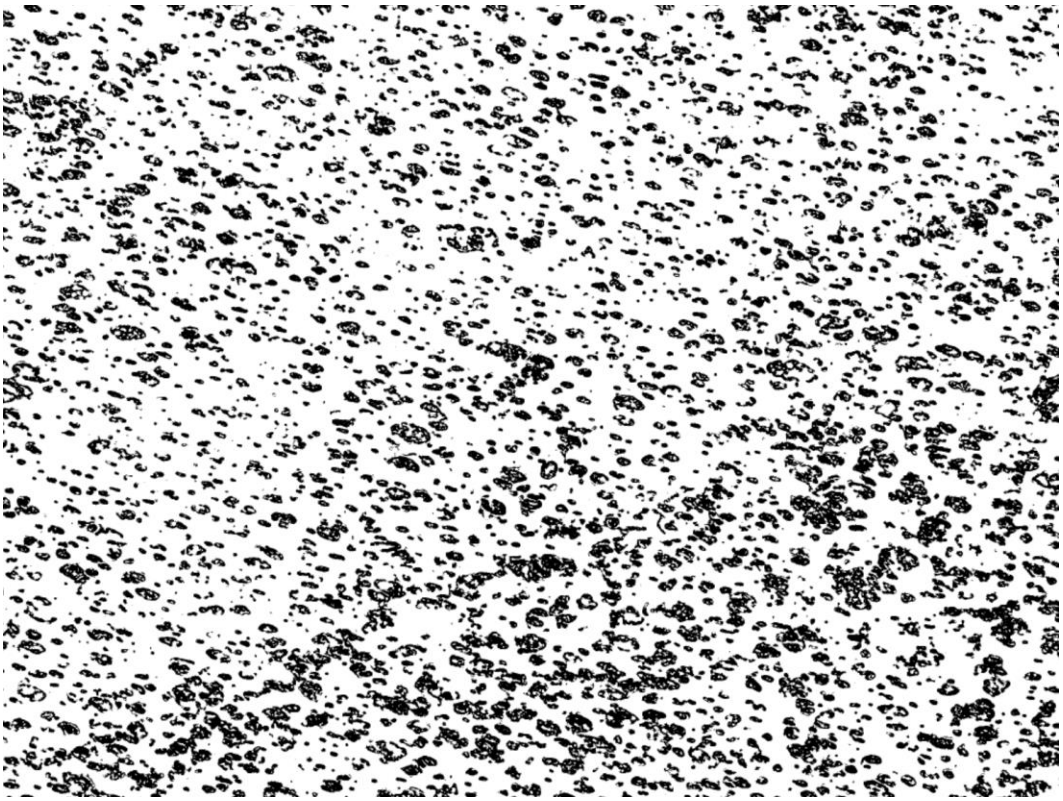


Figure S11: Binary image representation of Figure 6b. Image has been processed to remove noise to ensure the best representation of the original image.

CONCLUSION

1. Two deodorized lignin samples were compared with two non-deodorized lignin samples all obtained from the Kraft pulping process. The differences found between the samples are minimal. The greatest difference between the deodorized samples and non-deodorized samples is the C-O-C stretching of the ether groups and C-O stretching of the G ring due to the removal of guaiacol and 4-ethyl guaiacol units during the deodorization process.
2. The tanδ value decreased with increasing lignin loading, indicating the material's decreased ability to dissipate energy upon impact. This was confirmed by the decreasing Izod impact resistance of the material with increasing lignin loading.
3. Both tensile and flexural moduli increased upon lignin addition due to lignin's reinforcing effect. However, the ultimate strain for both the tensile and flexural tests decreased as the lignin loading increased.
4. Optical microscopy images show the agglomeration of lignin particles in VF35, which shows poor miscibility between lignin and ABS at higher lignin loadings.
5. Nanoindentation was completed on neat ABS, lignin-ABS blends, and lignin carbon fiber. Given the modulus of neat ABS and lignin carbon fiber, it was concluded that the rule of mixtures can be successfully used to predict the moduli of lignin-ABS blends at the microscale.

VITA

Neel Patel was born in Ahmedabad, India on October 26th, 1995, to Jayanti and Hansa Patel and has one brother, Jaymin. He grew up in India until he was seven years old, before coming to the U.S. In the U.S., he moved from one state to another several times, before his parents got a good job opportunity in Knoxville, TN in 2005. Neel graduated from Morristown East High School and completed his undergraduate degree in chemical engineering from University of Tennessee in 2019. After his undergraduate education, Dr. Dayakar Penumadu provided an opportunity to join his lab for the MS thesis. Since then, Neel's work has focused on working with Prisma Renewable Composites, LLC to characterize lignin-based composite materials. In his free time, Neel enjoys playing sports outdoors and reading books.